



$^{40}\text{Ar}/^{39}\text{Ar}$ geochronology at the Instituto de Geociências, USP: instrumentation, analytical procedures, and calibration

**PAULO M. VASCONCELOS¹, ARTUR T. ONOE², KOJI KAWASHITA²,
ADALBERTO J. SOARES³ and WILSON TEIXEIRA²**

¹University of Queensland, Department of Earth Sciences, Brisbane, Qld, 4072 Australia

²Universidade de São Paulo, Instituto de Geociências, Cidade Universitária, 005508-900 São Paulo, SP, Brasil

³Instituto de Pesquisas Energéticas e Nucleares, Cidade Universitária – USP, 005508-900 São Paulo, SP, Brasil

*Manuscript received on May 11, 2001; accepted for publication on December 24, 2001;
contributed by KOJI KAWASHITA* AND WILSON TEIXEIRA**

ABSTRACT

Laser heating $^{40}\text{Ar}/^{39}\text{Ar}$ geochronology provides high analytical precision and accuracy, μm -scale spatial resolution, and statistically significant data sets for the study of geological and planetary processes. A newly commissioned $^{40}\text{Ar}/^{39}\text{Ar}$ laboratory at CPGeo/USP, São Paulo, Brazil, equips the Brazilian scientific community with a new powerful tool applicable to the study of geological and cosmochemical processes.

Detailed information about laboratory layout, environmental conditions, and instrumentation provides the necessary parameters for the evaluation of the CPGeo/USP $^{40}\text{Ar}/^{39}\text{Ar}$ suitability to a diverse range of applications. Details about analytical procedures, including mineral separation, irradiation at the IPEN/CNEN reactor at USP, and mass spectrometric analysis enable potential researchers to design the necessary sampling and sample preparation program suitable to the objectives of their study.

Finally, the results of calibration tests using Ca and K salts and glasses, international mineral standards, and in-house mineral standards show that the accuracy and precision obtained at the $^{40}\text{Ar}/^{39}\text{Ar}$ laboratory at CPGeo/USP are comparable to results obtained in the most respected laboratories internationally. The extensive calibration and standardization procedures undertaken ensure that the results of analytical studies carried out in our laboratories will gain immediate international credibility, enabling Brazilian students and scientists to conduct forefront research in earth and planetary sciences.

Key words: geochronology, $^{40}\text{Ar}/^{39}\text{Ar}$ method, irradiation, calibration.

INTRODUCTION

Modern geochronology requires high analytical precision and accuracy, improved spatial resolution, and statistically significant data sets, requirements often beyond the capabilities of traditional geochronological methods. One of the most

significant advances in geochronology in the past decade has been the development and dissemination of fully automated laser heating $^{40}\text{Ar}/^{39}\text{Ar}$ analysis. The $^{40}\text{Ar}/^{39}\text{Ar}$ methodology, developed 35 years ago (Merrihue and Turner 1966), has gained enormous momentum in the past two decades with the increased availability of affordable laser extraction systems (Plieninger and Schaeffer 1976, York et al. 1981, Sutter and Hartung 1984) and with the dissemination of appropriate software for sample analysis

Correspondence to: Paulo Marcos Vasconcelos
E-mail: paulo@sol.earthsciences.uq.edu.au
Fax: 61-7-3365-1277

*Member of Academia Brasileira de Ciências

and data reduction (Deino and Potts 1990).

A newly commissioned $^{40}\text{Ar}/^{39}\text{Ar}$ dating laboratory at the *Instituto de Geociências* at University of São Paulo, Brazil is the first fully operational $^{40}\text{Ar}/^{39}\text{Ar}$ dating laboratory in South America. The recent construction of the $^{40}\text{Ar}/^{39}\text{Ar}$ laboratory facility at CPGeo/USP and the establishment of a cooperation agreement between USP and the *Instituto de Pesquisas Energéticas* (IPEN) (authorization CNEN/IPEN no. 1130/92), which facilitates the access of CPGeo/USP researchers to the IEA-R1 nuclear reactor at USP, provides the Brazilian geological community with a new powerful geochronological tool, adding to the already established methods of K-Ar, Rb-Sr, Sm-Nd, Pb-Pb and U-Pb.

In addition to its importance in academic research, the new facility at USP will promote greater interaction between industry and the university given that the $^{40}\text{Ar}/^{39}\text{Ar}$ methodology has important applications in minerals and energy resources exploration (Vasconcelos 1999a). The fully automated facility will provide high precision analysis on a timely basis, meeting the often rigid requirements of the mineral and oil exploration industry.

The $^{40}\text{Ar}/^{39}\text{Ar}$ geochronology method is a versatile tool suitable to the study of a diverse range of geological processes, such as chronology of volcanic processes (e.g., McDougall 1981, 1985, Renne and Basu 1991, Renne et al. 1992, 1997, Renne 2000); dating cooling rates in plutonic rocks (e.g., Harrison 1981); thermochronology of metamorphic terrains (e.g., Harrison and McDougall 1982, McDougall and Harrison 1999); thermochronology of shear zones (e.g., Goodwin and Renne 1991, Lee 1995, Dunlap 1997); dating of meteorites (e.g., Turner 1969, Podosek and Huneke 1973, McConville et al. 1988); chronology of tektites and impact events (e.g., Izett et al. 1991, Swisher et al. 1992, Culler et al. 2000); sediment provenance studies (e.g., Renne et al. 1990); dating of diagenetic processes (e.g., Girard and Onstott 1991, Smith et al. 1993, Onstott et al. 1997, Dong et al. 1995, 1997); dating of hydrothermal alteration in mineralized environments (e.g., Turner and Bannon 1992); and weath-

ering geochronology (e.g., Vasconcelos et al. 1992, 1994a, b, 1999a, b).

We will present below a full description of the new CPGeo/USP laboratory installations, equipment, analytical procedures, and results of calibration tests and analyses of standards. We will also discuss future developments for the laboratory.

LABORATORY CONSTRUCTION AND INSTALLATIONS

The CPGeo/USP $^{40}\text{Ar}/^{39}\text{Ar}$ laboratory had major funding from FAPESP through project 94/0678-4 “ $^{40}\text{Ar}/^{39}\text{Ar}$ methodology applied to the geodynamic evolution of Western Gondwana continent”. The project enabled importing the most advanced technology for the implementation of this dating technique in Brazil. Funding for the acquisition of instrumentation (i.e., mass spectrometer, laser, optical system, microscopes, computers, fume-hood, appropriate furniture, etc.) totaled US\$ 425.000. An additional R\$ 270.000, from FAPESP and PRONEX program 41.096.0899.00, were invested in infrastructure (e.g., UPS – uninterrupted power supply – systems, transformers, generator, water cooling tower, grounding and lightning protection, consulting, etc.). Project 94/0678-4 began in 1994 and required four years for completion. The long construction period resulted from the careful selection of the appropriate spectrometer, negotiations with suppliers in Europe, the long construction period for the equipment, refurbishment of the laboratory space at USP, delays in the acquisition of ancillary instrumentation, and bureaucratic delays in the acquisition and importing of the equipment.

The CPGeo/USP $^{40}\text{Ar}/^{39}\text{Ar}$ laboratory also underwent a long licensing process required by Norm 6.02 from the National Commission of Nuclear Energy (CNEN) for the irradiation of samples at IPEN and the manipulation of radioactive material. This licensing process required our research group to:

- determine the number of irradiations to be carried out each year, the duration of each irradiation, and the position in the reactor where the

irradiation should be carried out;

- devise appropriate means of sample encapsulation to avoid spilling samples in the reactor pool or contaminating the samples with reactor water;
- identify the radioisotopes produced during neutron activation of samples and standards;
- devise appropriate shielding for transferring, handling, and storing irradiated samples;
- equip the laboratory with proper signage and access restrictions required for safe handling of radioactive material;
- train the personnel responsible for the operation;
- license a technician in a Radioprotection Training Course for the preparation, use, and handling of radioactive sources;
- implement appropriate procedures in case of emergency.

After meeting all the requirements above, the $^{40}\text{Ar}/^{39}\text{Ar}$ laboratory received CNEN license No. AP-0869, which permits production and handling of small quantities of radioisotopes for research purposes.

Every stage of the project up to the testing stage in the first semester of 1999 received technical support from staff from the Berkeley Geochronology Center, Berkeley, Ca. The final tests, fine tuning, and implementation of the analytical procedures were conducted by the two senior authors. Researchers from CPGeo/USP (K. Kawashita, W. Teixeira, A. T. Onoe) briefly visited similar laboratories abroad to compare instrumentation and exchange information about technical procedures.

LABORATORY SIZE AND ROOM LAYOUT

The laboratory complex occupies an area of 48 m², divided into four interconnected rooms (Fig. 1): a temperature and humidity controlled room housing

the mass spectrometer and extraction line; a restricted access laboratory equipped with a microscope, fume hood, and a lead-lined cabinet for handling and storing radioactive samples; a sample preparation room for grain picking and loading irradiation disks; and a plant room housing two UPS units and transformers.

ELECTRICAL INSTALLATIONS

We designed and built the electrical installations at the $^{40}\text{Ar}/^{39}\text{Ar}$ laboratory at CPGeo/USP to provide clean and continuous power to all the instrumentation in the laboratory. The power supply to the electronic components was divided into two independent systems, precision electronics and power electronics, each equipped with its own UPS unit. The first system contains a 5 KVA, 220 V monophase Salicru UPS-5000-MI-CB that supplies power to the MAP-215-50 mass spectrometer, its electronic components, and a Keithley 6512 electrometer. The second system, equipped with a 30 KVA, 220V, three-phase Salicru UPS-30-3MI, supplies power to a Coherent Innova 90 plus Ar-ion laser, a Newport MM-3000 motion controller, one turbomolecular pump, two rotary pumps, two getter pumps, one Vac-ion pump, one ion gauge, one thermocouple gauge, two power Macintosh computers, two printers, a Sony television monitor and recorder, and the optical illuminators for the sample chamber.

Both UPS systems ensure uninterrupted and clean power, minimizing noise, current oscillations, and enabling continuous gas extraction and mass spectrometric analysis independently of interruptions to the external power supply. In case of major failure to the power supply to the building, a 150 KVA, 220V, three-phase diesel Stamac generator automatically switches on and provides continuous power to the laboratory and annexed facilities. Laboratory components not sensitive to momentary interruptions in the power supply, such as the air conditioning systems, Polycold cryocooling device, water pumps, laser refrigeration system, air compressor, fume hood exhaust system, and room lighting, draw their electricity from a circuit directly

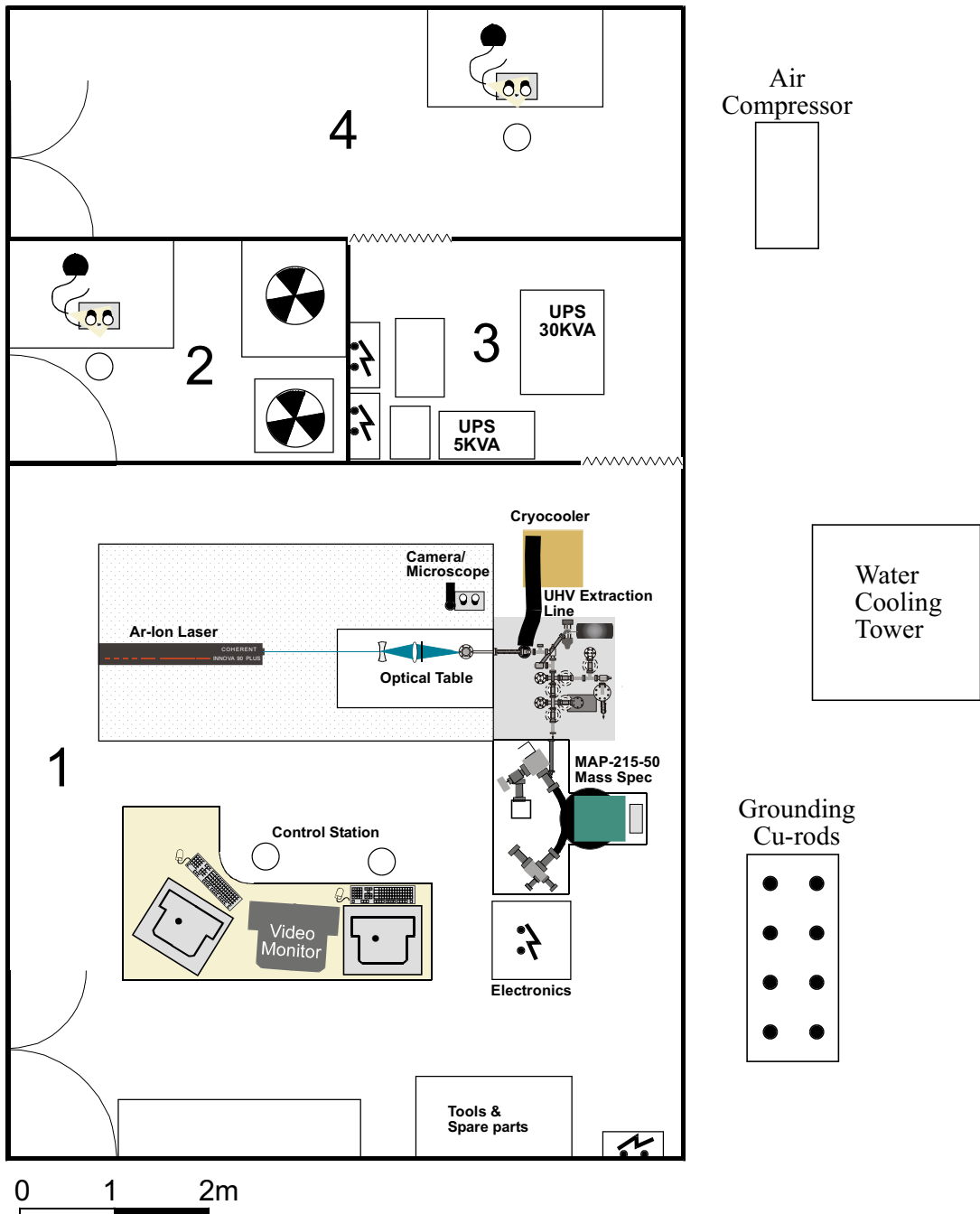


Fig. 1 – The CPGeo/USP ⁴⁰Ar/³⁹Ar Laboratory is divided into four main areas: (1) temperature and humidity controlled room housing the mass spectrometer, extraction line, and the control station; (2) laboratory equipped with a microscope, fume hood, and a lead-lined cabinet for handling and storing radioactive samples; (3) sample preparation room for grain picking and loading irradiation disks; and (4) plant room housing two UPS units and transformers. Air compressor, water cooling tower, and grounding Cu-rods are located in the external area adjacent to the laboratory.

linked to the diesel generator.

Finally, the laboratory is equipped with a certified grounding and lightning protection system that ensures safety of the equipment and operators and minimizes the effects of static charges, environmental perturbations, and telluric currents.

WATER INSTALLATIONS

The water installation circuit provides cooling to the laser system and getter pumps. It consists of a water cooling tower (ALPINA 4/2 W20-II-CENT) coupled to a centrifuge fan that promotes water/air heat exchange; two water pumps, operating in alternating cycles, to pressurize the system; metal and fiber water filters to ensure water cleanness; and a water circulation system in PVC pipes.

Since the flux and pressure required for cooling the getter pumps are low, the circuit is fed directly from the water tower, passing through a metal filter installed at the exit from the tower and returning directly to the tower reservoir. The laser, however, requires greater cooling capacity and clean water devoid of colloidal particles, microorganisms, and dissolved salts. To meet these requirements, laser refrigeration is achieved by re-circulating distilled water cooled through a water/water heat exchange unit (Coherent Laserpure 40). Continuous flow from the water cooling tower through the Laserpure cools the distilled water in the internal reservoir. Hot water exiting the Laserpure returns to the upper part of the water cooling tower and descends by gravity to the bottom reservoir exchanging heat with the atmosphere as it descends.

AIR CONDITIONING

Two of the four rooms in the $^{40}\text{Ar}/^{39}\text{Ar}$ laboratory complex require air-conditioning, particularly the mass-spectrometry room, where heat sensitive equipment such as the Hall probe and the electron multiplier are housed. The mass-spectrometry room is kept at $23 \pm 1^\circ\text{C}$ by two independent air conditioning systems (an 18.000 BTU/h Carrier Hi Wall and a 30.000 BTU/h Carrier Split Modernita). The room housing the UPS units and transformers is cooled by

a wall-mounted 18.000 BTU/h Springer Mondial air conditioning unit.

INSTRUMENTATION

The laboratory equipment can be divided into two major units: an ultra-high vacuum extraction line and the MAP-215-50 mass spectrometer (Fig. 1). A brief description of the extraction line and the mass spectrometer are provided below.

EXTRACTION LINE

The $^{40}\text{Ar}/^{39}\text{Ar}$ geochronology laboratory at USP is equipped with a home built fully automated noble gas extraction and purification system, illustrated in Figs. 2 and 3. The system is composed of an optical table, where sample visualization and gas extraction by a 6-W continuous Ar-ion laser occurs, and a stainless steel ultra-high vacuum (UHV) gas purification system equipped with a Polycold Cryocooler and two C-50 Fe-Ti-Zr SAES getters.

SAMPLE VISUALIZATION AND LASER OPTICS

Pure mineral grains or rock fragments are placed in a copper disk, loaded into the UHV sample chamber, and baked to $150\text{-}250^\circ\text{C}$ (Fig. 2). Several geometries for the sample disks are available, depending on the size and the number of samples to be analyzed. The most commonly used disks are 145-pit and 221-pit copper disks (Fig. 4). Once the samples have been loaded into the pits, the disk is placed in a stainless steel ultra-high vacuum sample chamber equipped with a 5-cm wide transparent silica window that permits viewing the interior of the ultra-high vacuum sample chamber (Fig. 2). This window also permits shinning a laser beam into the sample chamber. The laser beam is stationary and is focussed at the bottom of the central pit in the copper disk through a divergent and a convergent lens system and a 45° mirror, as illustrated in Fig. 2. The convergent lens is mounted on a moveable stage driven by a Newport 850F linear actuator controlled via a Newport MM3000 motion controller. Movement of the stage along the beam path permits

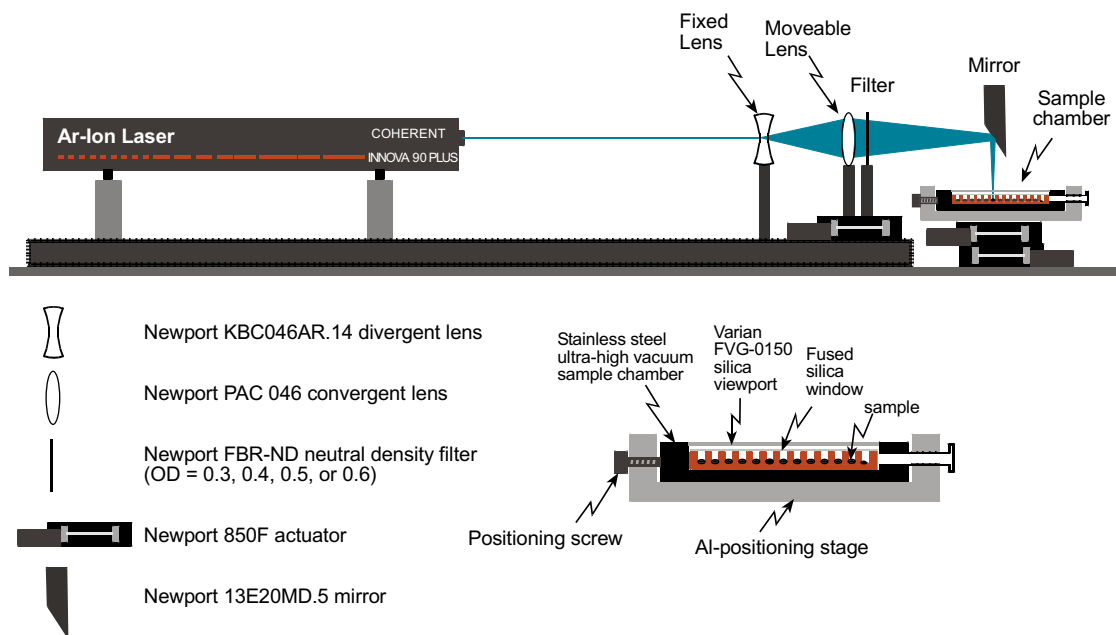


Fig. 2 – Schematic diagram illustrating the main optical components in the laser-heating and sample visualization line. The diagram also illustrates the ultra-high vacuum sample chamber where single crystals or rock fragments are inserted; the sample chamber moves on computer controlled linear actuators allowing the grains in the sample chamber to be positioned directly under the stationary laser beam.

focussing or enlarging the beam at the bottom of the pits in the sample disk (Fig. 2).

Every pit in the copper disk can be placed directly under the laser beam by moving the sample chamber, which sits on a moveable stage driven by two Newport 850F linear actuators computer controlled via the Newport MM3000 motion controller. Total travel distance is 50 mm in the x and y directions, which permits exposing all pits in the copper disk to the laser beam (Fig. 2).

The samples in the sample chamber are directly monitored on a SONY 21" Trinitron video screen (Fig. 1). Image is captured via a Digital CCD camera mounted on an Opto binocular microscope aligned at 90° to the direction of the laser beam. An image of the sample pit is reflected into the camera through a 45° front surface Al-coated mirror (Fig. 1). The image is illuminated through a light source emitting from the microscope. Direct monitoring permits evaluating the behavior of the sample dur-

ing heating and also permits the whole heating operation to be remotely controlled or recorded on tape or DVD for future studies.

LASER HEATING

The composition of the sample chamber window limits the type of laser beam that can be used for gas extraction: silica window is transparent to Ar-ion lasers, but absorbs at the common operating frequency of CO₂ and UV lasers. We use a Coherent 6W continuous Ar-ion laser, which emits in the 480-540 nm wavelength. A focussed laser beam (beam diameter ca. 10-20 μm) is used to fuse the sample when total fusion analysis is desirable. The laser beam can also be calibrated and preset to desired beam diameter (e.g. 2 mm) which permits a large sample grain to be heated nearly homogeneously.

Two distinct modes of operation are possible with the extraction system: **total fusion**, when the laser output power is computer-driven to 3-6 W for

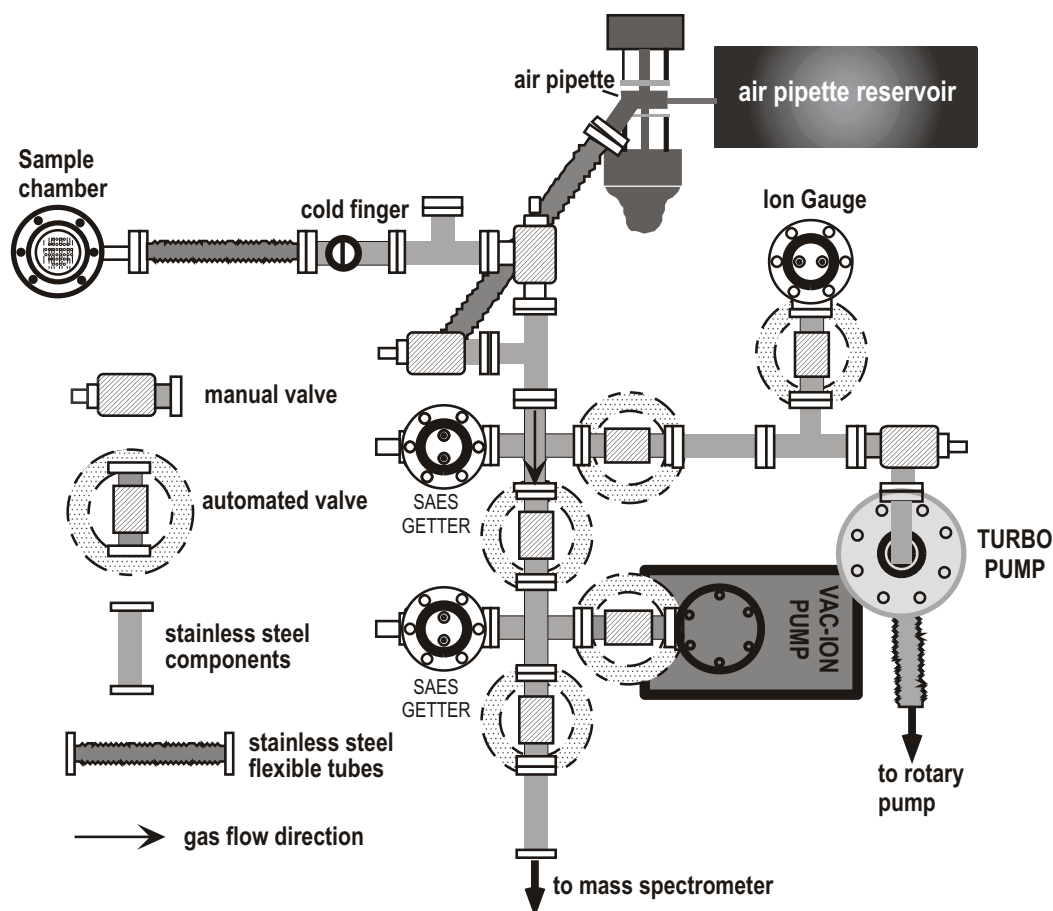


Fig. 3 – This diagram depicts the layout and the main components constituting the core of the ultra-high vacuum extraction line. All components are made of stainless steel and bakeable to 350-400°C.

10-30 seconds, the rock or mineral sample is heated to $\sim 1300 - 2000^\circ\text{C}$ and fuses, releasing all of its Ar content in a single step; and **incremental heating** (or **step heating**), in which the laser output power is computer-driven to a predetermined value, which depends on the nature of the mineral or rock under study, and maintained at that output intensity for 30-60 seconds. This procedure is repeated several times for a sample, at progressively higher laser output power. In the incremental heating method, several fractions of the Ar gas contained in a sample, extracted at progressively higher temperatures, are analyzed. Laser output power and the number of steps to be analyzed depend on the nature, size, age, and K-content of the sample, the desired resolu-

tion appropriate for the study, and the sensitivity and resolution of the mass spectrometer where the gas will be analyzed. If a laser energy output resolution greater than that possible with the laser control is desired, neutral density filters can be placed between the divergent and convergent lenses to increase attenuation of the laser beam (Fig. 2).

GAS PURIFICATION

The gas extracted from a sample must be stripped of all active gases (N_2 , O_2 , CO_2 , H_2 , H_2O , hydrocarbons, etc.) before mass spectrometric analysis. Purification is achieved by allowing the gas to flow through a series of cleaning devices mounted in an ultra-high vacuum stainless steel extraction

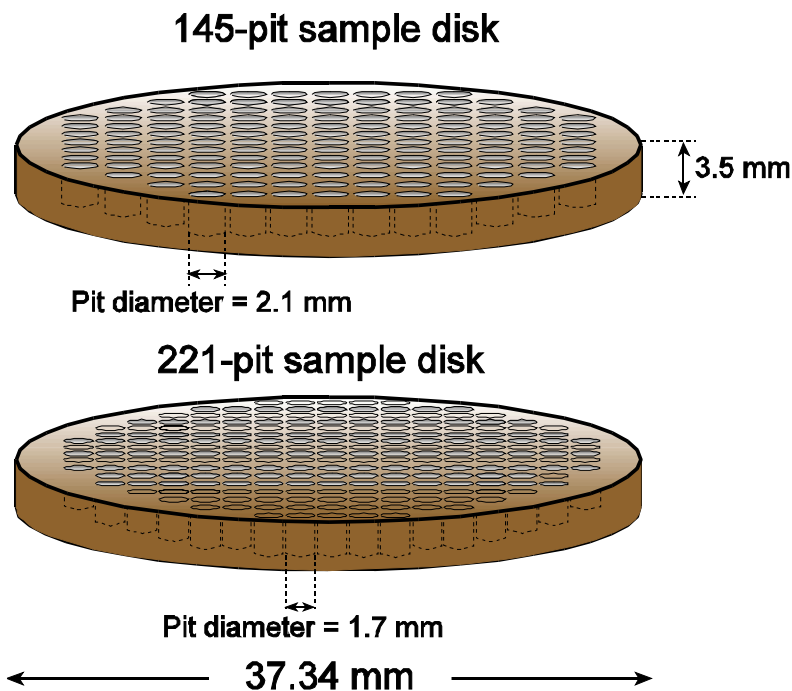


Fig. 4 – The sample disks routinely used at the CPGeo/USP $^{40}\text{Ar}/^{39}\text{Ar}$ Laboratory contain either 145, 2.1 mm wells, or 221, 1.7 mm wells, imposing a limit on the largest single crystals or rock fragments (2.1 mm) analyzed by the laser heating method. The analysis of larger grains, although possible, requires specially made sample disks.

line. Ultra-high vacuum in the extraction line is achieved and maintained through a VARIAN Turbo-V7LP pump backed by an Edwards E2M5 rotary pump, a VARIAN Noble Diode Vac-Ion pump and two SAES GP50 getter pumps, as illustrated in Fig. 3. The rotary pump is isolated from the turbo pump by an Edwards FL20K filtering system and a Edwards BRV-10MK isolation valve to prevent catastrophic oil vapor back-flow into the ultra high vacuum extraction line in the case of turbo pump failure. Extraction line pressure is monitored through a VARIAN UHV-24 nude ionization gauge mounted at the exit of the extraction system. The ultra-high vacuum line is equipped with a number of manual and computer controlled valves that allow the flow of gas through the system to be predetermined and remotely controlled, and total extraction line volume is 406 cc.

Gases extracted from mineral/rock samples expand into the first stage of the extraction line by flowing through a hollow stainless steel tube partially obstructed by a vertical internal wall (cold finger). The gas must flow through the tip of the tube, which is cooled to -132°C through the use of an external Polycold cryocooling device (Fig. 1). The cold finger helps to freeze CO_2 , H_2O , hydrocarbons and other active gases, but does not impede the passage of noble gases. Any remaining active gas not trapped by the cold finger is cracked and adsorbed onto a SAES C-50 getter cartridge operated at 2.2 A ($400\text{-}500^\circ\text{C}$) (Fig. 3). After 1-5 minute cleaning time, the gas is automatically allowed to expand into the second stage of the extraction line, also equipped with a SAES C-50 getter cartridge operated at 25°C to ensure complete removal of active gases (Fig. 3). After an additional 2-5 minute

cleanup time, the gas is allowed to expand into the mass spectrometer. Equilibration time is 45s, after which mass spectrometry starts.

MAP-215-50 MASS SPECTROMETER

The Mass Analyser Products (UK) MAP-215-50 mass spectrometer at USP is a 15-cm radius with extended geometry and 50mm 90° sector electrostatic analyzer equipped with a Nier-type source (Nier 1940), which ensures high sensitivity and resolution (Fig. 5). The mass spectrometer houses two independent collectors, a Faraday collector positioned on the high-mass side of the optic axis and a Balzers 217 electron multiplier positioned on the low-mass side (Fig. 5). A fixed collector slit enables mass resolution of ca. 440-450 (10% valley), allowing the resolution of all argon peaks from their nearest-neighbor hydrocarbon interferences, making it ideally suited for analyzing small gas volumes.

The mass-spectrometer vacuum is achieved and maintained by an Leybold TRIVAC E D2,5E rotary pump, a VARIAN 30 Ls⁻¹ Triode ion pump, and a SAES GP50 getter pump equipped with a C-50 cartridge. A foreline MDC KMST-100-2 trap and a Leybold MD-16 manual valve placed between the rotary pump and the mass spectrometer prevent oil back flow into the spectrometer. The ion and getter pumps are isolated from the source through VARIAN all metal valves. The valve isolating the Triode ion pump from the source (Fig. 5) has been automated in-house to permit remote control through pneumatic-driven linear actuators, enabling full automation of the mass-spectrometric analysis.

The mass spectrometer is directly linked to the extraction line through a stainless steel inlet tube (Figs. 1 and 5). The volume in the mass spectrometer-inlet tube assembly is isolated from the extraction line through a pneumatic controlled valve. An additional all-metal mini-valve between the mass spectrometer and the inlet tube permits completely closing the spectrometer from the external environment in case of emergency. The mass spectrometer -inlet tube volume is 1390 cc, which ensures that 77% of the gas volume extracted from

the sample and purified in the extraction line expands into the mass spectrometer, minimizing uncertainties due to kinetic-dependent mass discrimination of Ar isotopes.

At installation, mass spectrometer sensitivity was 8.6×10^{-4} amps.torr⁻¹, ^{40}Ar rise rate was 3.6×10^{-6} A.min⁻¹ (ca. 8.7×10^{-13} cc.min⁻¹) and resolution was 446, with the mass spectrometer operating at 3kV and 200 μA trap current. Since the signals shown in this study were measured in the electron multiplier, but sensitivity calculations were carried out in the Faraday detector, it is useful to know the relative signals between the two detectors. The feedback resistor used in amplifiers for the Faraday detector is $10^{11}\Omega$ and feedback resistor for amplifiers in the electron multiplier is $10^9\Omega$; operating gain in the multiplier relative to the Faraday detector was 1.2×10^4 .

Periodic scans, from mass/e 3 to 60, in dynamic and static modes, provide information on the cleanliness of the system. Representative scans are shown in Fig. 6.

AUTOMATION

The laboratory is fully automated through Mass Spec v. 5.11, a Macintosh MS Basic software written specifically for $^{40}\text{Ar}/^{39}\text{Ar}$ analysis and data reduction (Deino 1996, unpublished software manual). A schematic illustration of the automation interface at the USP laboratory is shown in Fig. 7. Full automation is possible because the extraction line and the mass spectrometer are equipped with remotely controlled pneumatic-actuated valves. The sequence of programmable steps in fully automated mode depends on the type of analysis to be carried out: mass spectrometer blank, full system blank, air pipette, or unknown analysis. A brief description of each type of analysis and automation procedures during gas extraction and purification are described below. Mass spectrometric procedures are the same for all types of analyses and will be described subsequently.

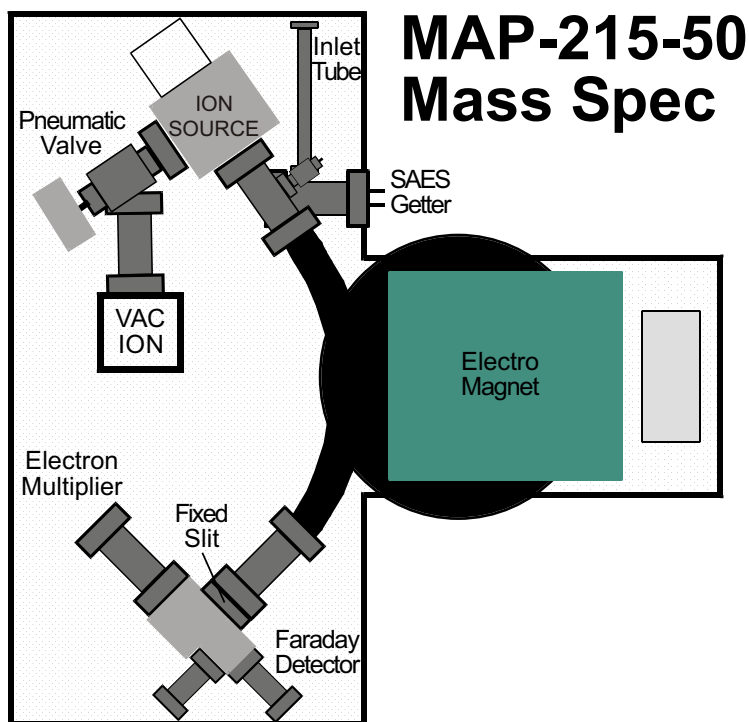


Fig. 5 – The schematic diagram of the MAP-215-50 noble gas mass spectrometer used at USP illustrates the relative positions of the sample inlet, the ionizing source, and the detectors. A pneumatically driven valve separating the source from the VAC-ION pump permits full automation of sample analysis. Up to 221 samples can be pre-programmed and run in fully automated mode.

MS BLANK

At the CPGeo/USP $^{40}\text{Ar}/^{39}\text{Ar}$ laboratory, MS blanks are measured every time a new sample disk is loaded for analysis and the extraction line is baked-out (approximately once a month). Valve positions and cleaning times at each stage are illustrated in Fig. 8.

FULL SYSTEM BLANK

High resolution $^{40}\text{Ar}/^{39}\text{Ar}$ geochronology depends on accurate measurement of Ar isotope ratios. To ensure accurate measurement of the relative volumes of Ar isotopes extracted from a sample, the masses of each Ar isotope present in the extraction line and mass spectrometer (full system blank) must be subtracted from the mass of these isotopes measured in a sample. This information is obtained by measur-

ing the amount of each Ar isotope accumulated in the extraction line and the mass spectrometer when the whole system is kept in static mode for the same period of time used when cleaning a fraction of gas extracted from a sample (typically 2-10 minutes). The steps in full system blank analysis and the positions of the valves in each step are shown in Fig. 9.

At the CPGeo/USP $^{40}\text{Ar}/^{39}\text{Ar}$ laboratory, we measure full system blanks immediately before and immediately after a mineral/rock grain is analyzed; we also program full system blanks during a mineral/rock analysis, depending on the type of material to be analyzed and the amount of gas expected from the grain. In special circumstances, we may program a full system blank between each step of a sample if the amount of gas is expected to be very low or very high or if we desire to monitor the vari-

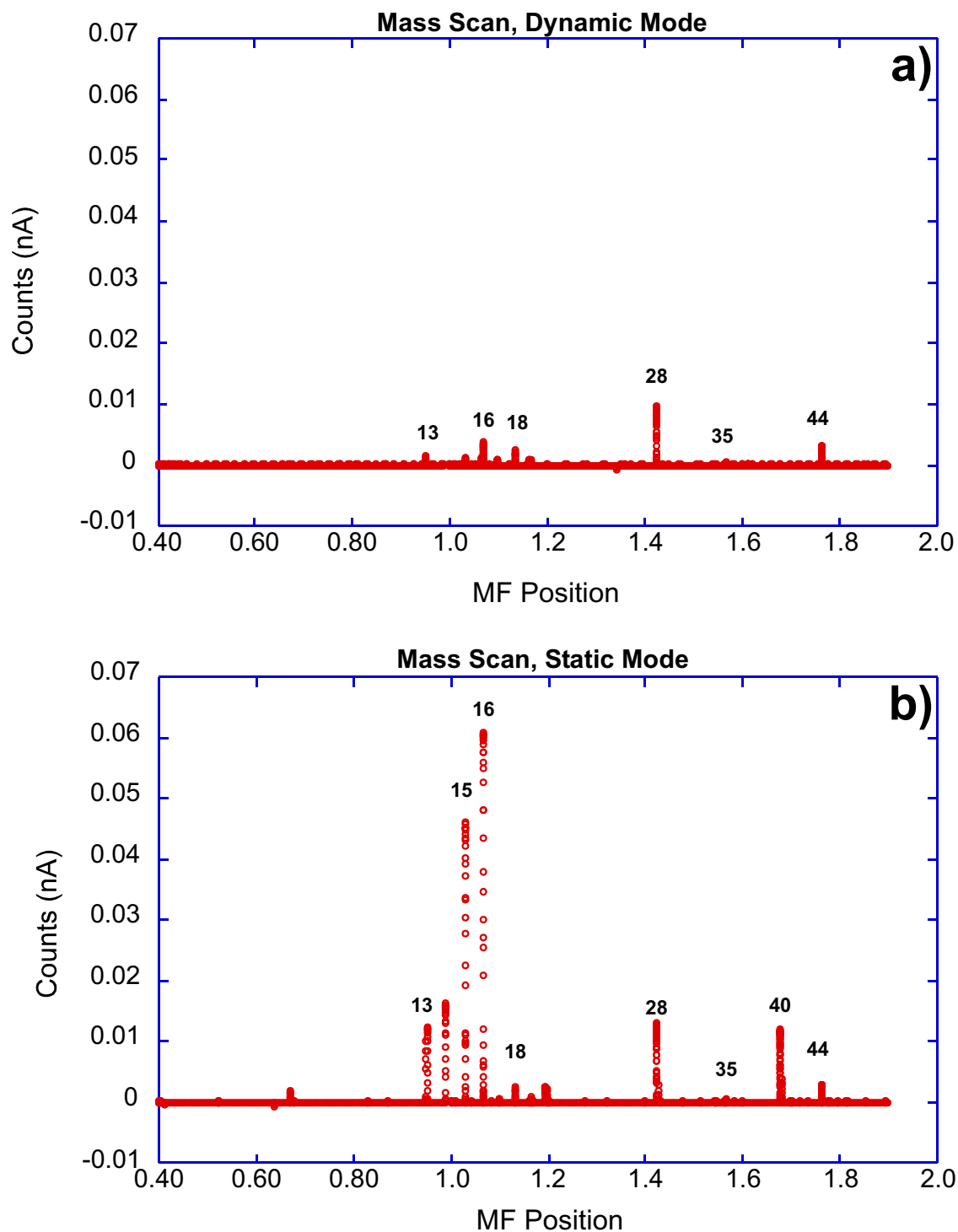


Fig. 6 – Continuous scans, from m/e 3 to 44, in dynamic (a) and static (b) modes, illustrate the low blanks achieved in the USP extraction line-mass spectrometer assembly. Scans were controlled by incrementally changing the magnetic field (MF) position.

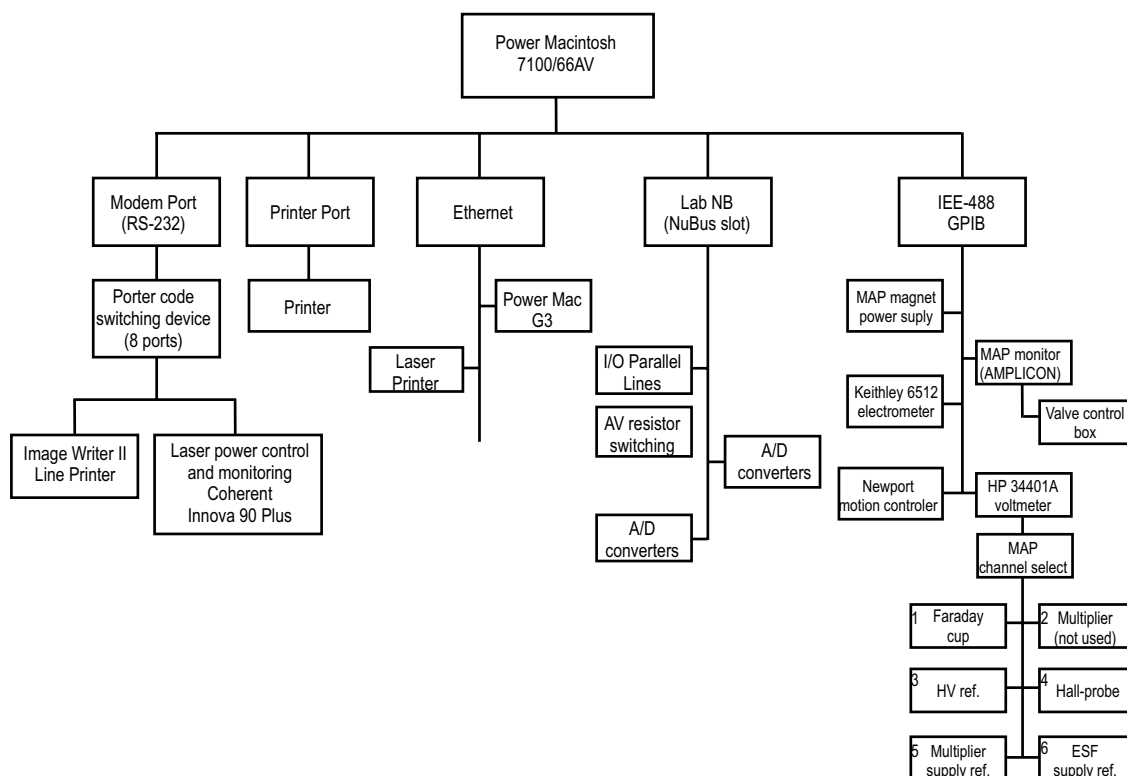


Fig. 7 – Full automation of the system is achieved using the software Mass Spec run (Deino 1996, unpublished software manual) on a Power Macintosh 7100 computer. The system permits automated laser operation, gas extraction and purification, mass spectrometric analysis, and data reduction, interpretation, and plotting. The whole system can be remotely operated via the internet, and it has been routinely run from Australia during the past year, making telechronology a common procedure at the CPGeo/USP $^{40}\text{Ar}/^{39}\text{Ar}$ Laboratory.

ation in the system blank during the gas extraction procedure. Blank values fall quickly after bake-out and the system is ready for analysis within a day after exchanging sample disks. Figure 10 illustrates the behavior of the blanks in the system at the USP laboratory.

AIR PIPETTE

To measure mass spectrometer sensitivity, a known amount of gas must be introduced into the mass spectrometer and the intensity of the signal measured in the Faraday detector. At the USP $^{40}\text{Ar}/^{39}\text{Ar}$ laboratory, we introduce 0.2 cc of purified air from an air pipette (containing approximately 1.2×10^{-13} moles of Ar) extracted from a 2-liter reservoir attached to the ultra-high vacuum extraction line (Fig.

3). Figure 10 illustrates the intensity of the signal obtained from an air pipette at the USP laboratory.

Air pipettes are also used to calculate Ar isotope mass discrimination due to kinetic effects, ionization efficiency, electron multiplier mass dependent response, etc. (McDougall and Harrison 1999, p. 88). An air pipette is measured between each sample and the discrimination (D) value is calculated according to the equation below

$$D = [R_t/R_m]^{1/\Delta M}$$

where R_t is the true value of the isotope ratio, R_m is the measured value of the isotope ratio, and ΔM is the mass difference between the two isotopes (Renne 2000). The calculated D value is entered into the preferences file for the Mass Spec program, enabling

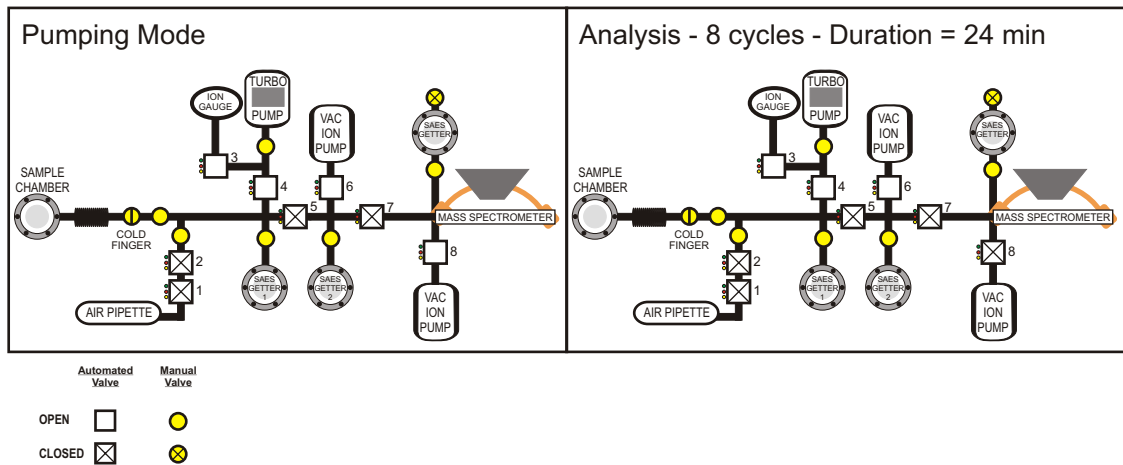


Fig. 8 – Diagrammatic illustration of the analytical steps, valves layout, and duration of each procedure during the analysis of a MS blank. Total duration of a MS blank analysis is approximately 24 min.

automatic correction for mass discrimination effects during sample analysis.

Valve positions and cleaning times at each stage during air pipette analyses are illustrated in Fig. 11. Figure 12a illustrates the $^{40}\text{Ar}/^{36}\text{Ar}$ values measured for a series of air pipettes (in excess of 500) analyzed at the USP laboratory. The results indicate that the ratios are relatively constant at ca. 289 (average = 289.14 ± 10.86 , for $n = 731$, which includes outliers; and average = 289.48 ± 2.17 , for $n = 723$, when outliers associated with operating errors are deleted), similar to measurements for this parameter carried out in other laboratories and resulting in the discrimination factors illustrated in Fig. 12b.

UNKNOWN

During sample analysis, each grain in the sample disk is pre-programmed for gas extraction. Sample pit position, laser output power, laser beam diameter, laser rise rate and time at full intensity, and gas clean-up time are programmed for each grain. After extraction from the grain, the gas expands through the cold finger into the first stage of the sample chamber. Valve positions and cleaning times for each stage are illustrated in Fig. 13.

During gas extraction we attempt to devise a

heating schedule that ensures, for each step, the release of gas volumes comparable with the gas volumes introduced by an air pipette. This procedure ensures that the discrimination correction deduced from the air pipette measurements is applicable to the gas samples. We have demonstrated, however, that gas samples ranging from 1/50 to approximately 20 times the volume of an air pipette do not show volume dependent discrimination and are suitable for analysis in our system. The lowermost values measurable depend on system blanks, and signals 5-10 times above blank values are suitable for analysis.

Figure 10 illustrates the range in gas volumes extracted during the analysis of a sample disk containing single crystals of Fish Canyon sanidine standards of variable grain sizes. A sample/blank ratio of 10:1 is desirable for precise analysis, but smaller signals can be reliably measured. Figure 14 illustrates the range of sample signals measured for gases extracted during the analysis of grains of feldspar, biotite, muscovite, and phlogopite of variable sizes and ranging in age from 80-1900 Ma. All samples were analyzed by the incremental heating method, one air pipette was analyzed between each sample grain, and a blank was analyzed between every two

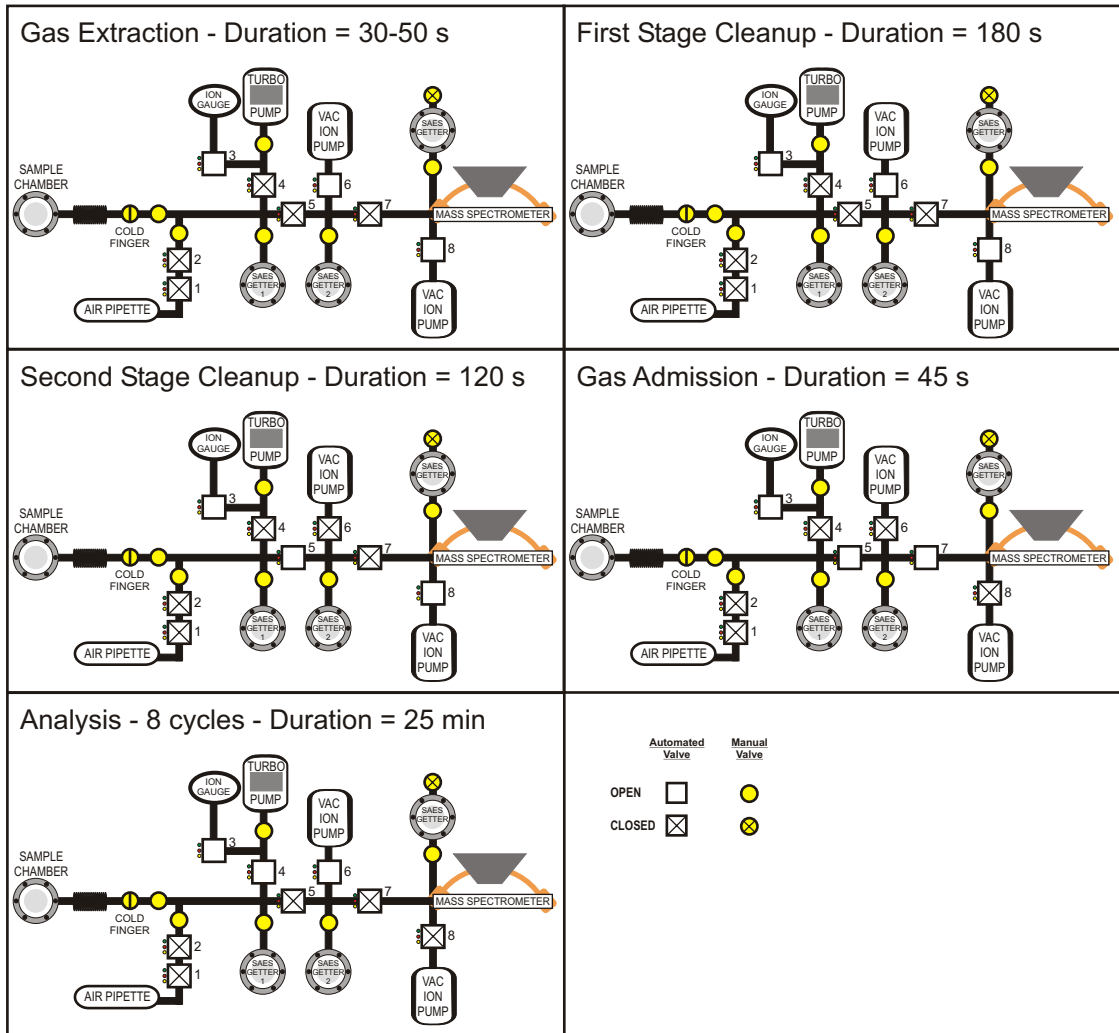


Fig. 9 – Diagrammatic illustration of the analytical steps, valves layout, and duration of each procedure during the analysis of a full system blank. Total duration of a full system blank analysis is approximately 28 min.

steps of the unknowns. The data in Fig. 14 display a large range in the size of the gas fraction extracted from samples during incremental heating analyses and also illustrate clearly the variation in the full system blank during sample analysis. Immediately after a large signal, the blank will rise momentarily (memory effects) but will quickly fall as sample analysis progresses. The results also show that during laser-incremental heating analysis is not always possible to ensure that a step will release sufficient gas for successful analyses. The unknown steps be-

low the dashed line in the diagram generally yield poorly defined apparent ages.

MASS SPECTROMETRY

Mass spectrometric analysis is fully automated and is carried out by the peak hopping method, where mass/e positions 40, 39, 38, 37, 36, and baseline at 36.2 and 35.8 are measured (Fig. 15). As soon as a gas fraction enters the mass spectrometer, the computer drives the magnet to the position of the last isotope measured in the previous cycle, mass/e 36,

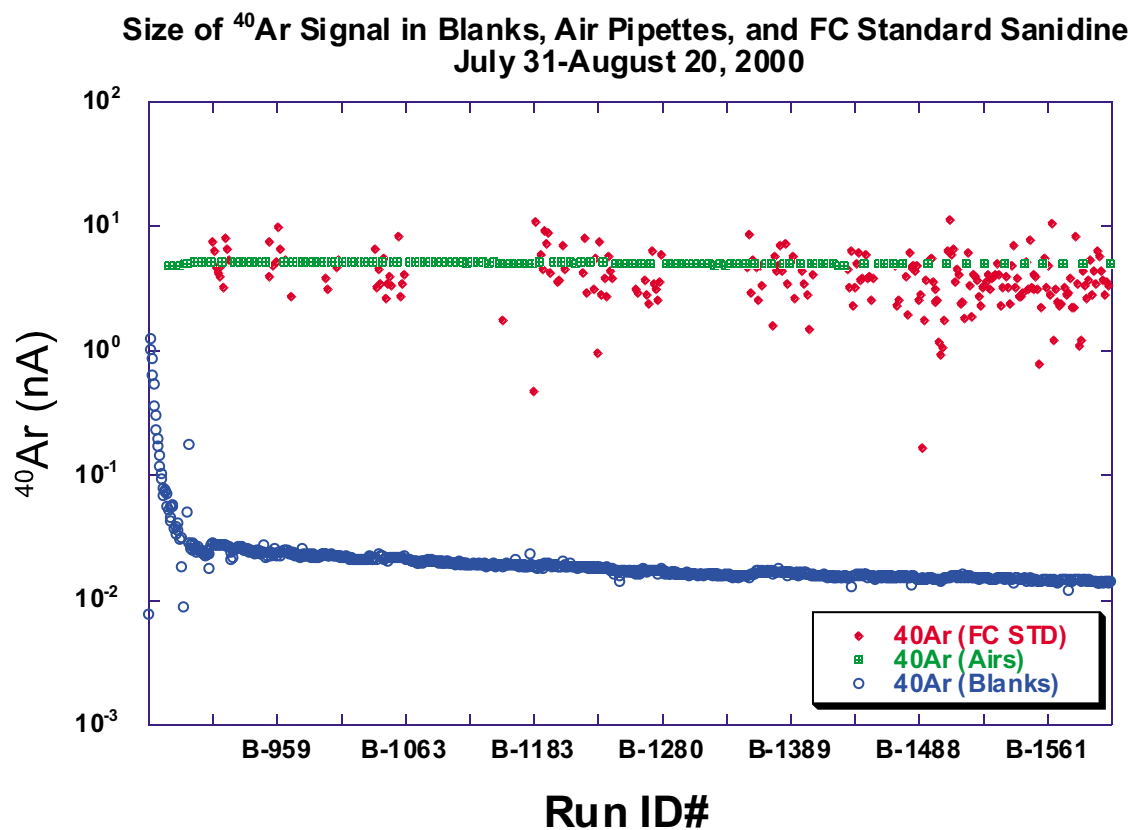


Fig. 10 – This plot illustrates the size of the ^{40}Ar signal (in nA of current measured in the electron multiplier) obtained for blanks, air pipettes, and grains of Fish Canyon sanidine standards analyzed at the USP laboratory. Notice the rapid decrease in the blank values immediately after bake out of the extraction line and the more gentle but continuous decrease in blank values. Air-pipette signals remain relatively constant throughout the analysis of a sample disk. The variation in the intensity of the ^{40}Ar signal obtained from single crystals of Fish Canyon sanidine standards illustrates the range of signals that can be accurately measured in our system.

to minimize hysteresis effects and then to the position corresponding to the middle of the ^{40}Ar peak top. After 45 seconds, valve # 7 closes and a ^{40}Ar peak auto-centering procedure ensures that the exact location of the center of the ^{40}Ar peak is determined. This auto-centering procedure permits correcting for minor drifts in the magnetic field. After auto-centering on mass/e 40, the system measures the baseline at positions 36.2 and 35.8 to account for detection system noises.

The magnetic field position for the ^{40}Ar peak top is updated into the MF Table and the positions for mass/e 39, 38, 37, and 36 are automatically updated. A cycle is completed by measuring mass/e

39, 38, 37, and 36. To ensure precision, the signals at mass/e 40, 39, 38 and 37 are measured 7 times (integration times of 0.35s with 5 integrations per displayed count) and the signal at mass/e 36 is measured 25 times. Five to ten cycles are measured for each fraction of gas extracted (Fig. 15). Once the 5-10 cycles, from mass/e 40 to 36, are complete, the baseline at mass/e 36.5 is measured again. These measurements are extrapolated to time zero (time of gas inlet into the mass spectrometer) and the extrapolated values are used in age calculation (Fig. 15).

An important parameter during mass spectrometry is the shape of the signal intensity for each isotope vs. time curve (isotope evolution). Linear or

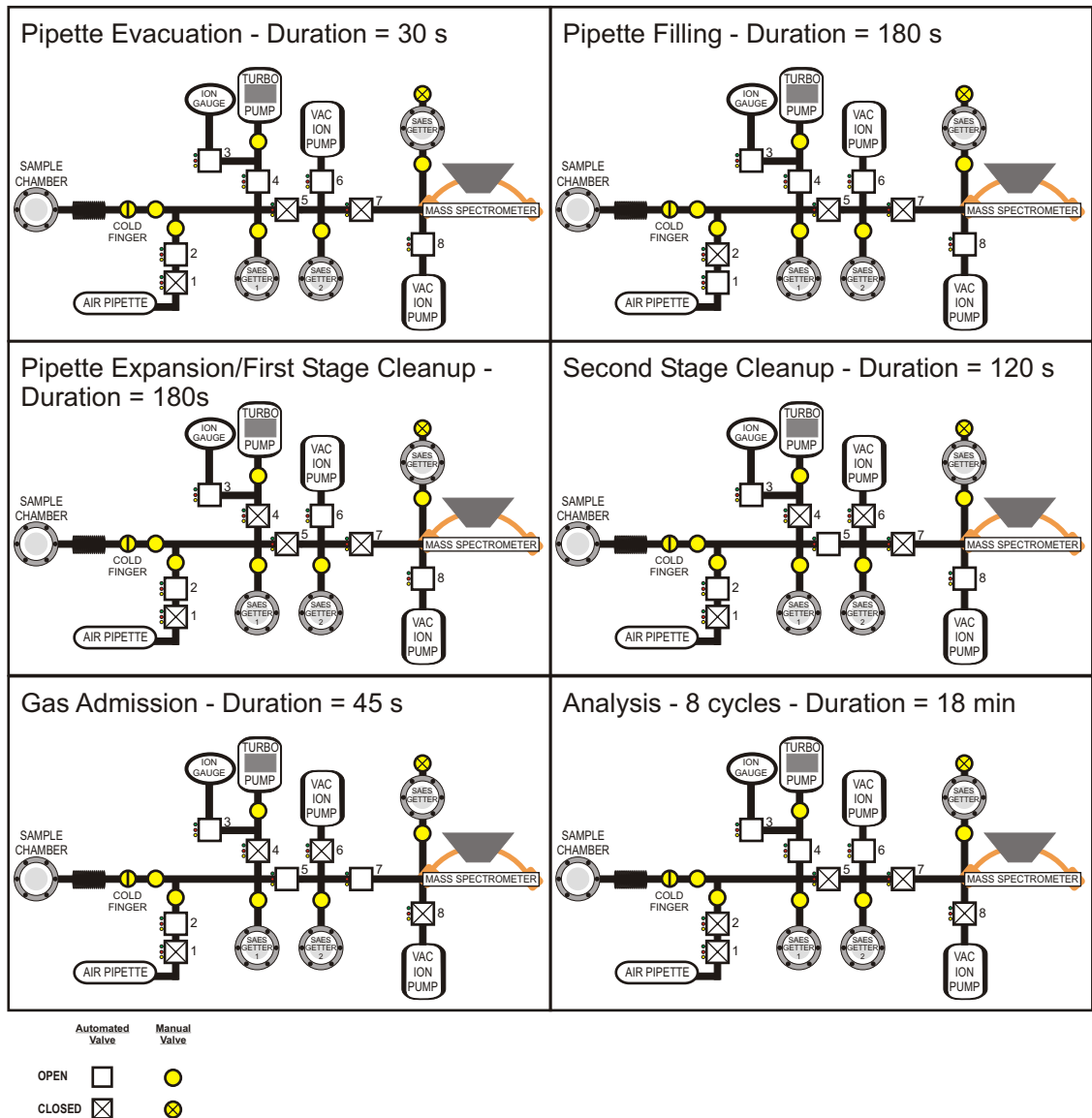


Fig. 11 – Diagrammatic illustration of the analytical steps, valves layout, and duration of each procedure during the analysis of an air pipette. Total duration of an air pipette analysis is approximately 28 min.

slightly parabolic isotope evolutions permit precise and accurate extrapolation to time zero. Figure 15 illustrates typical evolutions for a blank, a sanidine standard, and an air pipette analyses at the USP lab. The nearly linear evolutions obtained suggest that the gas allowed into the mass spectrometer is suitably clean. Evolutions that deviate from linear or slightly parabolic curves indicate peak suppression in

the mass spectrometer source, a phenomenon generally associated with the presence of active gases (i.e., H_2) or large volumes of He (Renne 2000) in the ionization source. Figure 16 illustrates evolutions for single grains of USGS muscovite standard P-207 (Dalrymple and Lanphere 1969) with and without the use of the cryocooler. The peak suppression noticeable in the first column, but absent in the second,

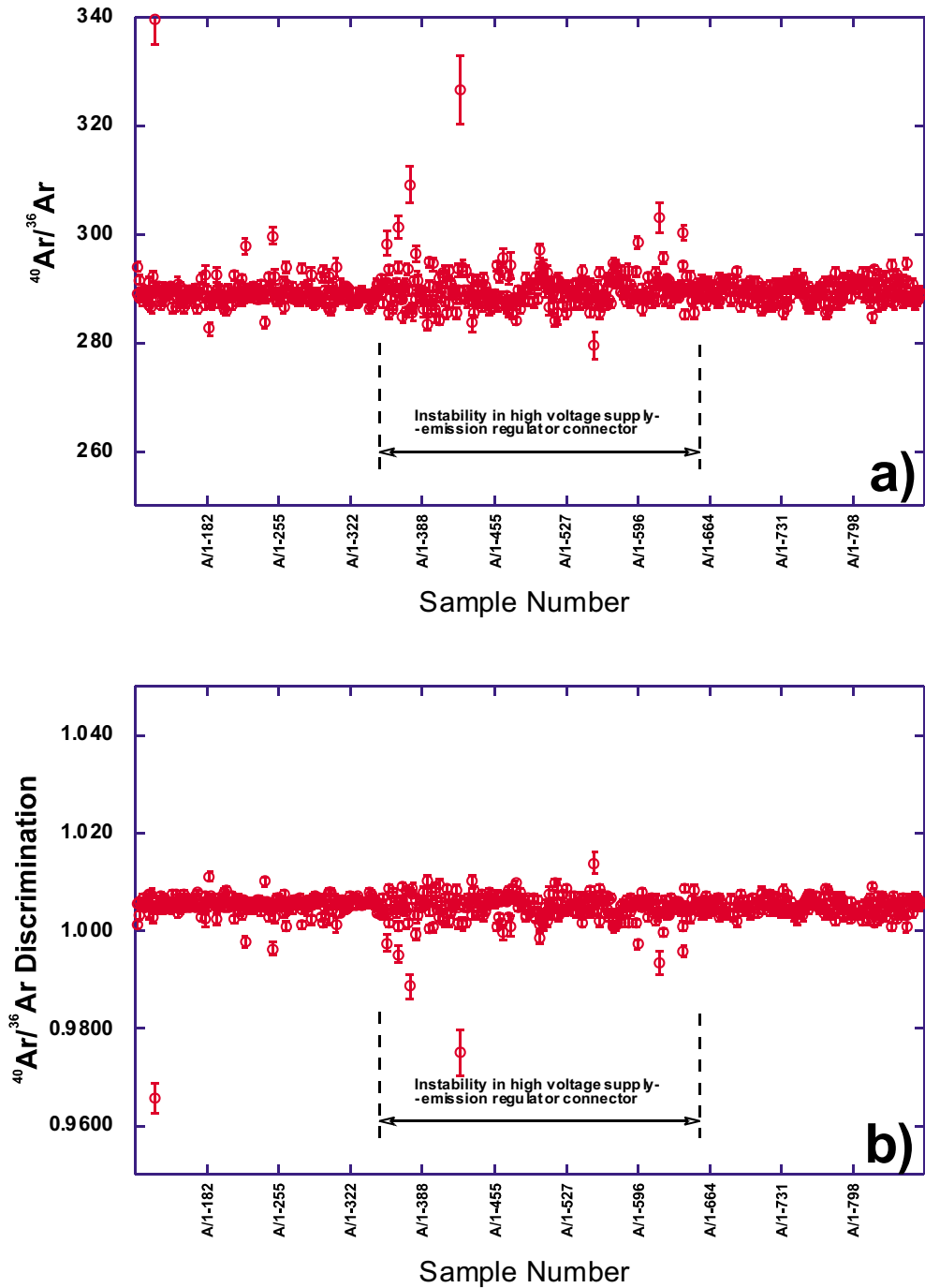


Fig. 12 – Figure 12a illustrates the $^{40}\text{Ar}/^{36}\text{Ar}$ values obtained from the analysis of air pipettes during an eight-month period. The ratios measured are relatively stable, except for a period when a loose connector between the emission regulator-high voltage supply introduced some noise in the system. Once this problem was resolved, the air pipette $^{40}\text{Ar}/^{36}\text{Ar}$ values stabilized at ca. 289. The $^{40}\text{Ar}/^{36}\text{Ar}$ values result in the discrimination values illustrated in Fig. 12b.

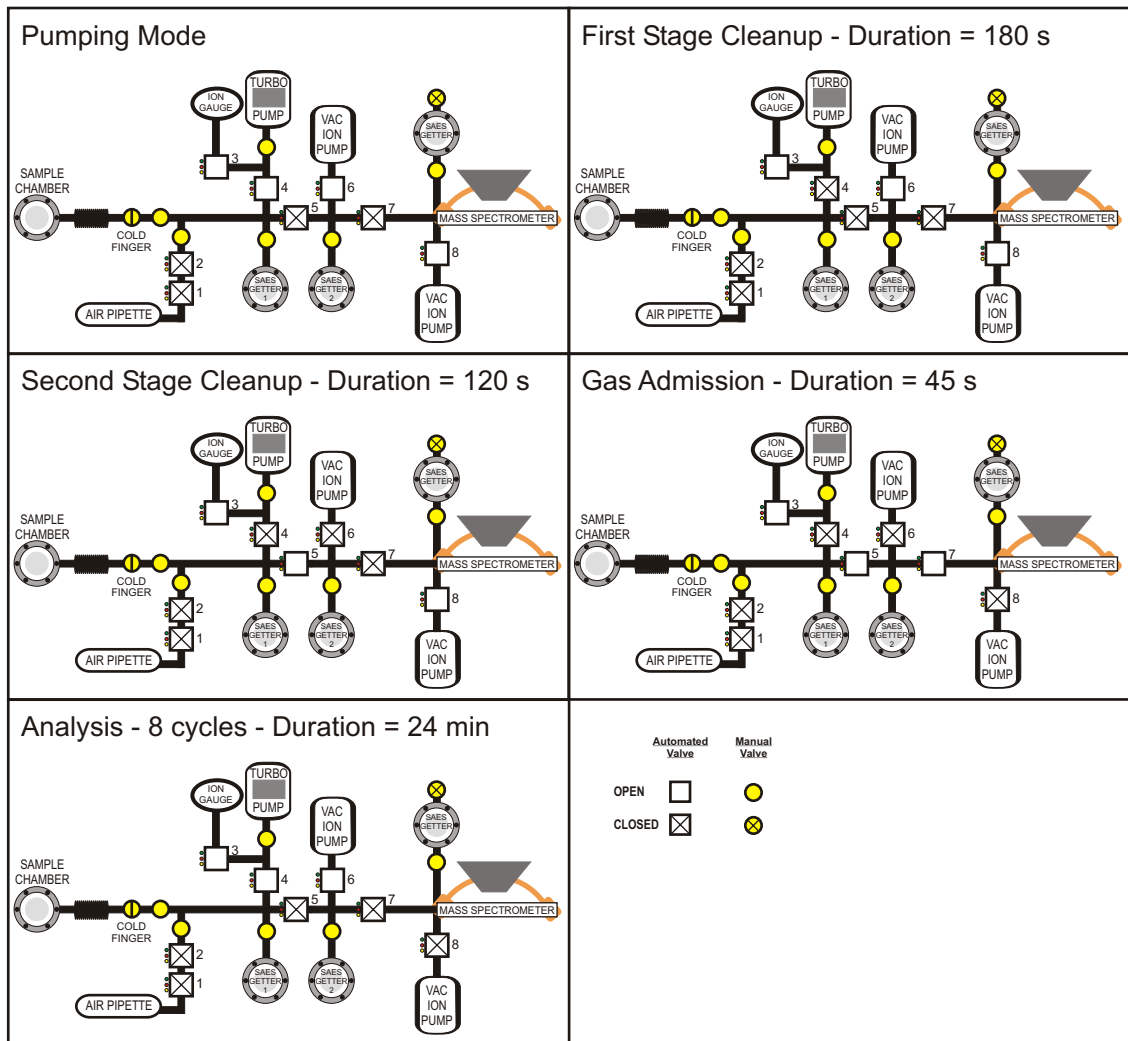


Fig. 13 – Diagrammatic illustration of the analytical steps, valves layout, and duration of each procedure during the analysis of a unknown sample. Total duration of each analysis is approximately 32 min.

attests to the effectiveness of the cryocooler as a gas purification device.

ANALYTICAL PROCEDURES

The versatility of the $^{40}\text{Ar}/^{39}\text{Ar}$ methodology provides several options for sample analysis: **total fusion** of mineral/grain separate, **incremental-heating gas extraction** (Turner 1969, Reynolds and Muecke 1978) of mineral/grain separate, or **in situ total fusion** (Sutter and Hartung 1984).

The **total fusion** method and the **in situ fu-**

sion are fast and permit dating many grains from the same sample. However, a total fusion $^{40}\text{Ar}/^{39}\text{Ar}$ analysis is equivalent to a K-Ar analysis. The total fusion method does not provide information on a sample's Ar retention properties, the presence of multiple generations or contaminants, and the possible Ar and/or K losses and gains by the sample. In situ laser fusion analysis presents several other complications. Generally, in situ analysis is desirable in polished thin sections, where the mineral to be analyzed has been petrographically described (Dong et

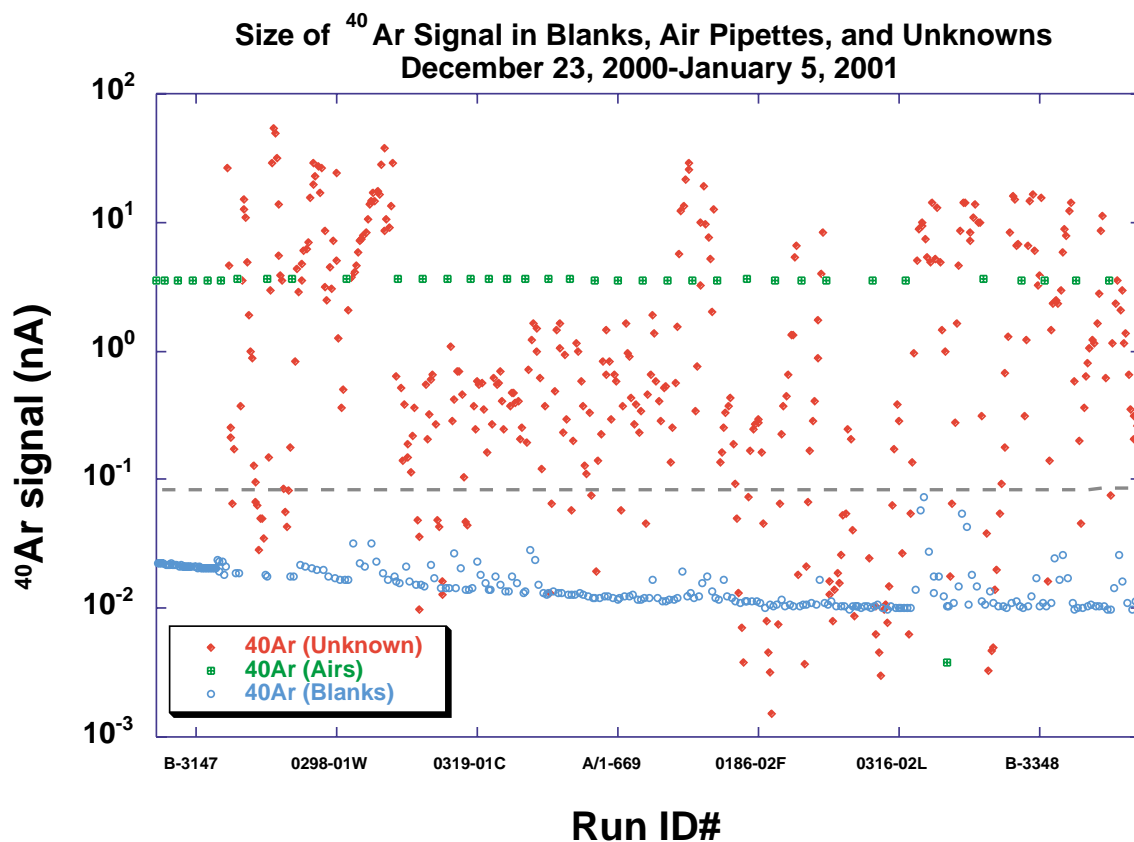


Fig. 14 – This series of blanks, air pipettes, and unknown analyses illustrate the behavior of blanks and air pipettes throughout the analysis of disk of samples. It is possible to notice the stability of the air pipette signals and the progressive decrease in the system blank with time, except for momentary increases in blank levels immediately after a large sample signal (memory effects). The figure also illustrates the large dynamic range of signals measurable in the system (10^{-3} to 10^2 nA of current in the multiplier). The values plotted below blanks identify instances in which the laser output power programmed for a step was insufficient to extract any gas from the sample or instances in which the sample heated was already completely degassed. In these cases, subtraction of the blank values from the small signals measured results in values plotting below the blank line. The dashed line illustrates the approximate desirable minimum value of ^{40}Ar necessary for accurate and precise analysis. Signals similar or slightly above blank values generally result in imprecise results.

al. 1997). Irradiation of odd shape samples, such as thin sections, requires special procedures for placing flux monitors as close as possible to the grain to be analyzed. The large sections irradiated also require special sample handling devices in the sample chamber. Finally, thin section sized-samples increase the background in the sample chamber/extraction line. For the reasons above we do not routinely carry out in situ laser fusion.

The main types of analyses performed at the CPGeo/USP $^{40}\text{Ar}/^{39}\text{Ar}$ laboratory are total fusion and incremental heating analysis of single grains, grain clusters, or rock fragments. Total fusion analysis are ideal for clean, single phase, homogeneous grains with a simple thermal history, when the distribution of radiogenic $^{40}\text{Ar}^*$ and neutron induced ^{39}Ar is expected to be uniform throughout the grain. We have so far restricted the single fusion method

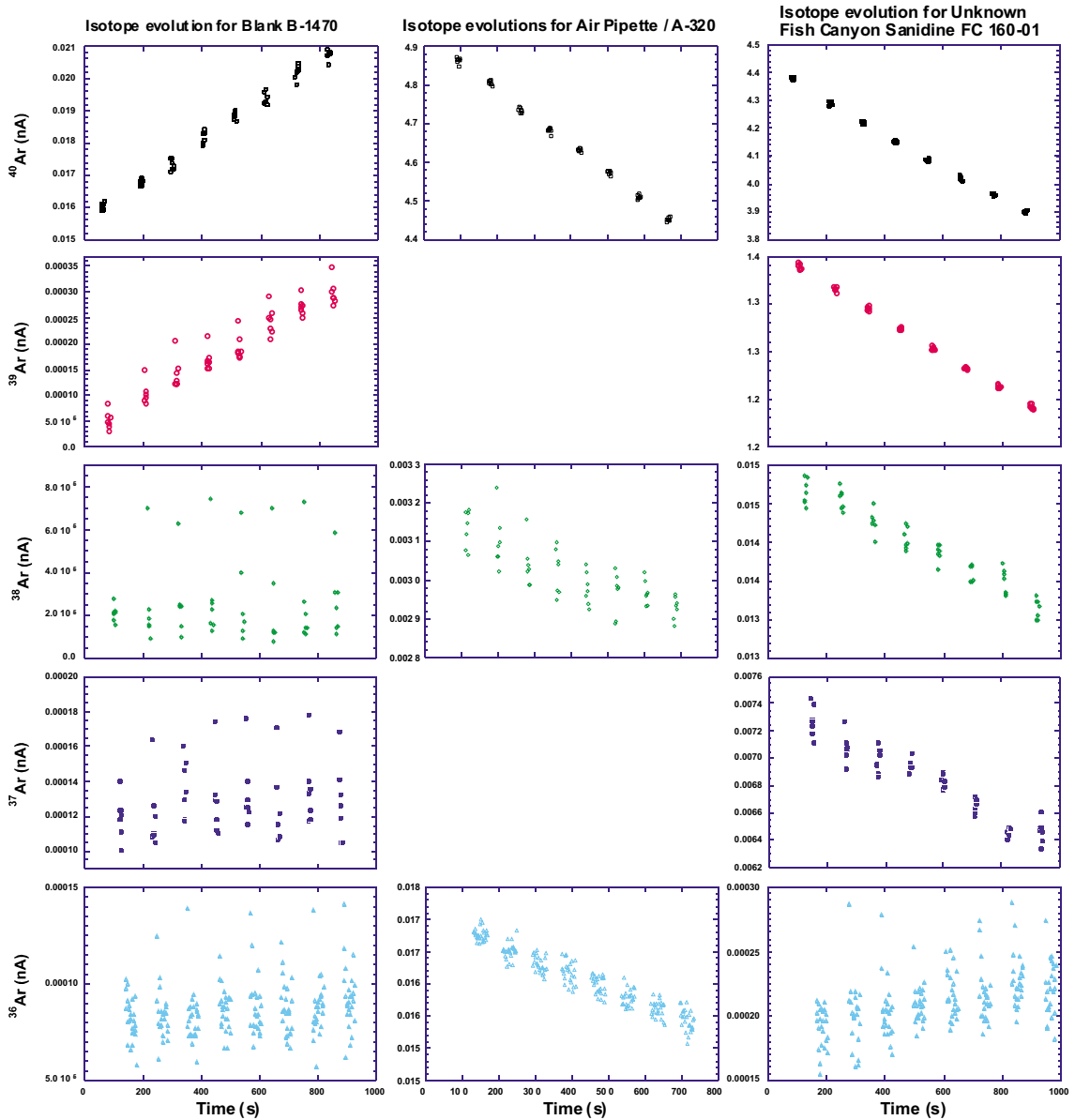


Fig. 15 – The isotope signal vs. time curve (isotope evolution) illustrated in this figure show the generally linear or slightly parabolic curves obtained in the MAP-215-50 spectrometer. The curves also illustrate the typical ascending evolutions for blanks and descending evolutions for stronger (air pipettes or unknowns) signals. Each cluster of points identifies a cycle. Several measurements of the top of the peak for each mass/e position (7 measurements for mass/e 40, 39, 38, and 37 and 25 measurements for mass/e 36) at each cycle improve the precision of the analyses. The measurement of several (5–10) cycles for each isotope ensures greater precision when extrapolating the values measured to time zero, which is the value used in age calculation.

to the analysis of standards, which, in general, meet the requirements above.

The incremental heating method is our chosen

procedure for unknown analysis. The incremental fusion method, however, requires effective coupling between the sample and the laser, which is a func-

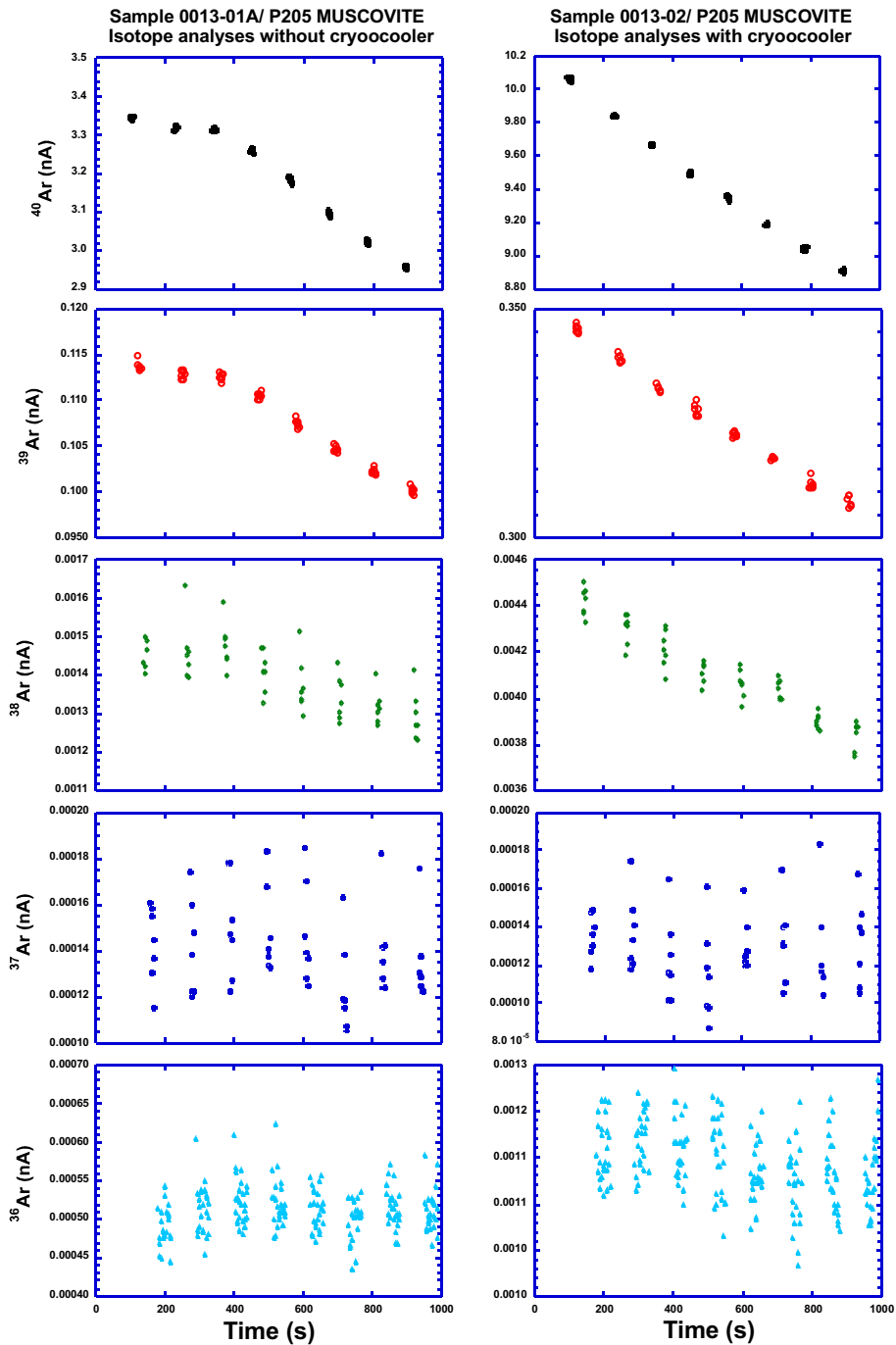


Fig. 16 – The evolutions in the first column correspond to a gas fraction from a hydrous sample (P-207 muscovite) analyzed without the use of the Polycold cryocooler in the extraction line. The second column illustrates evolutions for the gas fraction extracted from another P-207 muscovite grain, this time using the cryocooler to trap active gases and water. The peak suppression observed in column one, and generally associated with the presence of active gases (H_2 , O_2 , N_2 , CO_2 , H_2O) in the mass spectrometer source, is absent in the second column, attesting to the effectiveness of the cold finger.

tion of the laser wavelength and the crystal bond vibration frequency. Most minerals/rocks couple well with Ar-ion lasers. However, optically transparent Fe-poor silicates such as quartz and alkali-feldspars, particularly sanidine, do not couple well, precluding their analysis by the incremental heating method. Coupling between these crystals and Ar-ion lasers in total fusion analyses is ensured by the addition of a dark glass made under high vacuum conditions (zero-age glass or ZAG).

SAMPLE PREPARATION

Sample preparation procedures must take into consideration the type of material (rock, sediment, weathering profile, etc.) to be analyzed and the objective of the project. Only grains smaller than 2.1 mm are analyzed by the laser-heating method at the CPGeo/USP laboratory, since 2.1 mm is the maximum diameter of the wells in the sample disks routinely used (Fig. 4). Grains in the **0.2–2.0 mm** range are ideal for $^{40}\text{Ar}/^{39}\text{Ar}$ analysis using the laser-heating method. Samples larger than 2.0 mm are difficult to heat homogeneously with the laser beam, and samples smaller than 0.2 mm may be difficult to manipulate.

When the desired phase is extremely fine grained, it is possible to load several individual crystals in the sample wells and heat these grains with a defocused laser beam. This procedure, however, suffers from the difficulty in ensuring that each grain in the copper well is evenly exposed to the laser beam, and it often results in heterogeneous heating of the sample. Spectra obtained when grains are heated to different temperatures may be difficult to interpret and, whenever possible, laser heating of several grains at the same time is avoided. Finally, the grain size should also be commensurate with the expected age for the sample: younger samples, relatively poor in $^{40}\text{Ar}^*$, require larger grains (1–2 mm); grains from older samples, rich in $^{40}\text{Ar}^*$, should be smaller (0.2–1.0 mm) to avoid creating large memory effects or overloading the electron multiplier.

When a properly equipped mineral separation laboratory is available, the samples can be submit-

ted to standard crushing and sieving procedures and pure mineral separates, in the desired size range, can be obtained. Alternatively, minerals can be extracted from desirable areas in the sample (alteration haloes in hydrothermal veins, growth bands in supergene minerals and ocean floor manganese nodules, etc.). To this end, sample preparation procedures should be compatible with the objectives of the study and the types of minerals available for geochronology. Detailed procedures for mineral separation for geochronology of volcanic rocks is given by Renne (2000). Vasconcelos (1999b) provides stepwise procedures for sampling and mineral separation for $^{40}\text{Ar}/^{39}\text{Ar}$ geochronology of weathering processes.

IRRADIATION

$^{40}\text{Ar}/^{39}\text{Ar}$ analysis requires the creation of Ar isotopes by neutron bombardment in a nuclear reactor. The irradiation is necessary because in the $^{40}\text{Ar}/^{39}\text{Ar}$ method, K is indirectly measured by the generation of the nucleogenic ^{39}Ar isotope by the reaction $^{39}\text{K}(n,p)^{39}\text{Ar}$ (Merrihue and Turner 1966) and time is obtained by the relationship:

$$t = (\lambda^{-1}) \cdot \ln[J \cdot ({}^{40}\text{Ar}^* / {}^{39}\text{Ar}_k) + 1]$$

where λ is the total decay constant for ^{40}K ($5.543 \times 10^{-10} \text{a}^{-1}$) (McDougall and Harrison 1999); λ_e is the decay constant of ^{40}K to ^{40}Ar ($0.5808 \times 10^{-10} \text{a}^{-1}$) (McDougall and Harrison 1999); ${}^{40}\text{Ar}^*$ is the total amount of radiogenic ^{40}Ar (obtained by subtracting the atmospheric ^{40}Ar and ${}^{40}\text{Ar}_k$ from the total amount of ^{40}Ar measured from the sample, where ${}^{40}\text{Ar}_k$ is the amount of ^{40}Ar generated by the reaction $^{40}\text{K}(n,p)^{40}\text{Ar}$); and ${}^{39}\text{Ar}_k$ is the amount of nucleogenic ^{39}Ar generated by the reaction $^{39}\text{K}(n,p)^{39}\text{Ar}$ (obtained by subtracting the ${}^{39}\text{Ar}_{Ca}$ from the total amount of ^{39}Ar measured from an aliquot of the sample, where ${}^{39}\text{Ar}_{Ca}$ is the amount of ^{39}Ar generated by the reaction $^{42}\text{Ca}(n,\alpha)^{39}\text{Ar}$).

J is a dimensionless irradiation parameter defined as

$$J \equiv ({}^{39}\text{K} / {}^{40}\text{K}) (\lambda / \lambda_e) \Delta \int \phi(E) \sigma(E) dE$$

where ^{39}K is the original amount of ^{39}K present in the sample; ^{40}K is the original amount of ^{40}K present in the sample; λ and λ_e are defined as above; Δ is the duration of the irradiation; $\phi(E)$ is the neutron flux at energy E ; $\sigma(E)$ is the neutron capture cross section at energy E for the reaction $^{39}\text{K}(n,p)^{39}\text{Ar}$.

The irradiation parameter J is determined by irradiating a neutron fluence standard of known age placed in the same irradiation container as the unknown. Measurements of the amounts of ^{40}Ar and $^{39}\text{Ar}_k$ produced in the standard provides the information necessary for calculating J :

$$J = (e^{\lambda t} - 1) / ({}^{40}\text{Ar}^* / {}^{39}\text{Ar}_k)$$

where t is the known age of the standard, determined independently; λ is defined as above; ${}^{40}\text{Ar}^*$ is the total amount of radiogenic ^{40}Ar measured from the standard; ${}^{39}\text{Ar}_k$ is the amount of nucleogenic ^{39}Ar generated by the reaction $^{39}\text{K}(n,p)^{39}\text{Ar}$ in the standard.

Measurement of ${}^{40}\text{Ar}^*$ and ${}^{39}\text{Ar}_k$ in the sample and standard requires correction for interfering isotopes created by the reactions $^{40}\text{Ca}(n,\alpha)^{36}\text{Ar}$, $^{40}\text{Ca}(n,\alpha)^{37}\text{Ar}$, $^{42}\text{Ca}(n,\alpha)^{39}\text{Ar}$, and $^{40}\text{K}(n,p)^{40}\text{Ar}$ (Brereton 1970).

IRRADIATION PROCEDURES

Samples (single crystal, cluster of crystals, rock fragment, glass, etc.) analyzed at the CPGeo/USP laboratory are irradiated, together with appropriate neutron flux standards, at the IPEN/CNEN IEA-R1 nuclear reactor. The samples and standards are placed into aluminum containers as illustrated in Fig. 17. Several standards are suitable as flux monitor and the choice of standard depends on the expected age for the sample to be analyzed. For young samples (< 4 Ma) we use the Alder Creek sanidine standard (1.186 ± 0.013 Ma) (Turrin et al. 1994). For samples in the 2–100 Ma age range, we use Fish Canyon sanidine, which has an age of 28.02 ± 0.09 Ma (Renne et al. 1998). For the 50–700 Ma interval we may choose to use biotite standard GA-1550 (MacDougall and Harrison 1999); however, we have adopted the 98.8 ± 0.5 Ma age for this standard as

proposed by Renne et al. (1998). For samples older than 700 Ma we use hornblende standard HB3gr (1079 ± 1 Ma) (Roddick 1983).

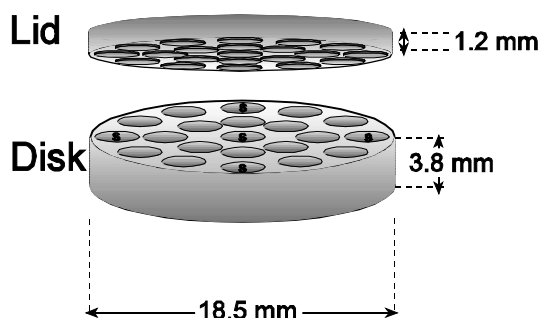


Fig. 17 – The irradiation disks used at the CPGeo/USP Ar Laboratory are made of 6063 T5 aluminum and are fitted with a lid to prevent sample cross-contamination. Neutron fluence monitor positions (S) are also illustrated in the diagram.

Once the sample and standards are placed in the correct positions in the irradiation disks (Fig. 17), the disks are closed with appropriate lids and individually wrapped with Al-foil. Individually wrapped disks are stacked and wrapped together with Al-foil and placed in a silica tube. This tube is sealed, ensuring that the samples are not exposed to excessive heating during encapsulation. The sealed vial is placed, through remote manipulation tongs, inside a 1.5 mm-wall Cd-container that is stored inside the reactor pool. The Cd-container is finally placed in a rotatable Al-rod and this rod is placed in the irradiation position 58–5 (Fig. 18), just outside the reactor core. After irradiation, the Cd-container is removed from the rotatable Al-rod, is remotely opened inside the reactor pool, and only the sealed Si tube is removed from the reactor pool. This procedure ensures that the sample is properly shielded from excessive thermal neutrons, it avoids handling of irradiated Cd (highly radioactive), and it also minimizes the risk of spilling samples in the reactor pool.

THE IEA-R1 NUCLEAR REACTOR AT IPEN/CNEN

The IPEN/CNEN reactor located at USP is a swimming pool reactor with 5 mega-Watts capacity cur-

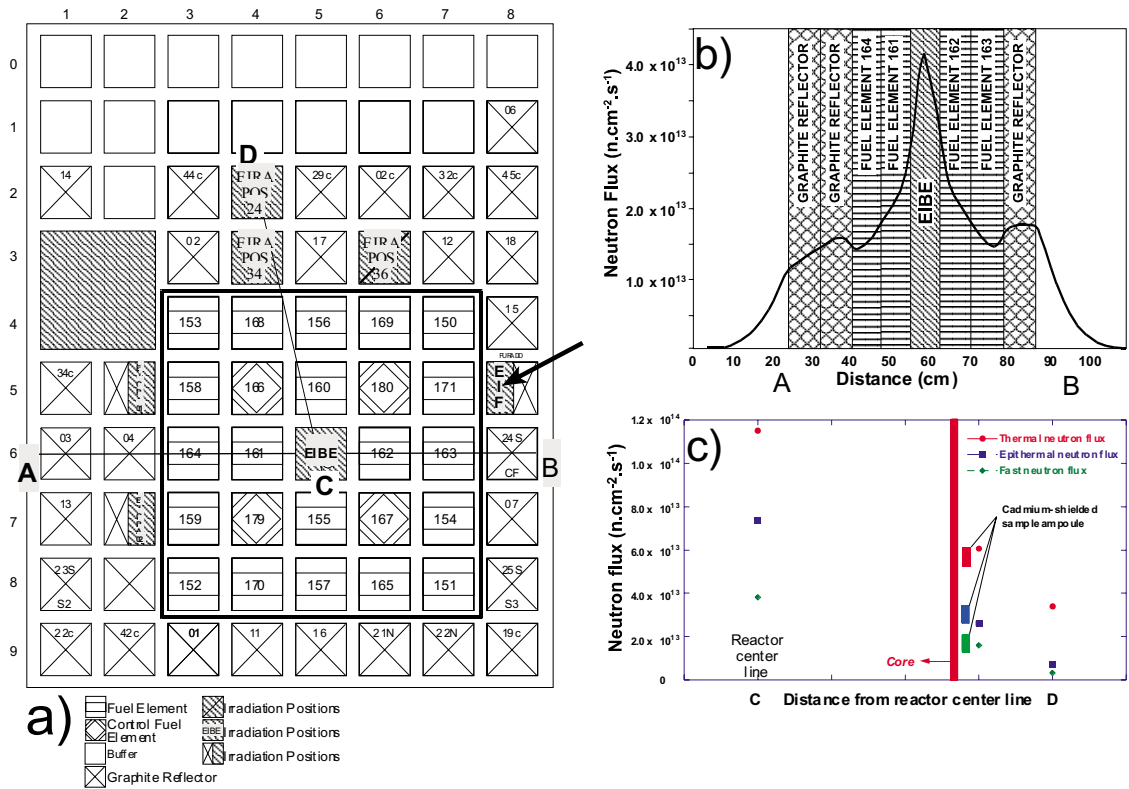


Fig. 18 – The IEA-R1 nuclear reactor at IPEN/CNEN uses 25 fuel elements (disposed in a 5 × 5 matrix as illustrated in (a)). The irradiation positions available (hatched areas) are mostly outside the core, which makes them subject to heterogeneous neutron fluxes. Position EIF58 (arrow) is the one currently used for irradiating minerals/rock samples for ⁴⁰Ar/³⁹Ar geochronology. Figure 19b illustrates the theoretical neutron flux in the reactor (A-B). The actual flux in irradiation positions EIBE, EIRA34, and EIRA24, EIF58 are illustrated in (c). The fluxes in these positions were determined by measuring the activities produced during the irradiation of gold foils with the reactor operating at 5MW.

rently operating at 2 mega-Watts. The reactor uses 24 fuel elements, composed of 18 plates of U₃Si₂Al e U₃O₈Al, arranged in a matrix of 5 × 5 elements, as shown in Fig. 18. The reactor core is surrounded by graphite reflectors and is water cooled. The reactor currently operates in 64-hour shifts (Monday morning to Wednesday night) imposing limits on the maximum duration of any continuous irradiation. The theoretical neutron flux in the reactor is illustrated in Fig. 18b. Experimental measurements of fast, epithermal, and thermal neutrons, using gold foil, at position 58–5 (and with the reactor operating at 5MW capacity) are ca. 1.7 × 10¹³, 2.9 × 10¹³, and 4.7 × 10¹³ n.cm⁻².s⁻¹ respectively (Fig. 18c),

placing the IEA-R1 reactor well within the neutron flux values of other reactors used in ⁴⁰Ar/³⁹Ar geochronology (McDougall and Harrison 1999, p. 56).

REACTOR CALIBRATION

Since the IPEN reactor has not been previously calibrated for ⁴⁰Ar/³⁹Ar geochronology, a series of tests are necessary to determine the appropriate irradiation procedures and correction parameters. To determine the horizontal variation in the neutron flux at the scale of a single irradiation disk (1.8 cm) and the precision with which the J-factor can be determined for a disk, Fish Canyon sanidine stan-

dards, arranged in a radial distribution in the irradiation disk as shown in Fig. 19, were irradiated for 24.6 hours. J-factors measured for the disk ranged from 0.001535 to 0.001790, yielding a mean value of 0.001635, standard deviation of 0.00013, and a coefficient of variation of 7.9% (Fig. 19), values unacceptable for precise and accurate $^{40}\text{Ar}/^{39}\text{Ar}$ analysis. The large range of J-values obtained for a single disk indicates that the horizontal heterogeneity in the neutron flux in the IPEN reactor is very large at the irradiation position used.

To circumvent this problem, a 30-hour irradiation was carried-out with the samples placed in a rotatable Al-rod driven by an external motor. The 9 m-long rod was inserted into the reactor position EIF58 and the samples were rotated during the irradiation. The rotational and precessional movements of the sample container inside the Al-rod ensures that each position in the irradiation disks receives the same neutron dosage, despite the heterogeneity intrinsic to the neutron flux. J-factors calculated from the analysis of a minimum of 10 grains of sanidine Fish Canyon standards from each well ranged from 0.004792 to 0.004828 (Fig. 19), yielding mean value of 0.00481, standard deviation of 0.0000095, and a coefficient of variation of 0.197% for the J-factor in a disk, parameters well suited for $^{40}\text{Ar}/^{39}\text{Ar}$ geochronology.

The discrepancy in J/hour values between the first and second irradiations arises from differences in the shelves where the samples were irradiated and not due to differences in reactor operating conditions. At both irradiations the reactor was operating a 2MW output. At 5 MW, the rapid neutron flux at shelf 1 is 1.891×10^{12} , while the flux at shelf 8 is $1.013 \times 10^{13} \text{ n.cm}^{-2}.\text{s}^{-1}$; samples positioned in different shelves within position EIF58 will be subject to neutron fluxes which may vary by up to a factor of 5.4.

Fish Canyon sanidine standards, arranged in radial geometry as shown in Fig. 17 and irradiated in ten different sample disks stacked into a vertical column, as illustrated in Fig. 20 (insert), were also analyzed. The vertical variation in neutron flux

measured is illustrated in Fig. 20. The results are comparable to similar tests carried out in the Oregon State University (USA) triga reactor (Vasconcelos, unpublished results), indicating that the vertical neutron flux does not pose problems for the sample sizes and the sample disks used in the USP laboratory.

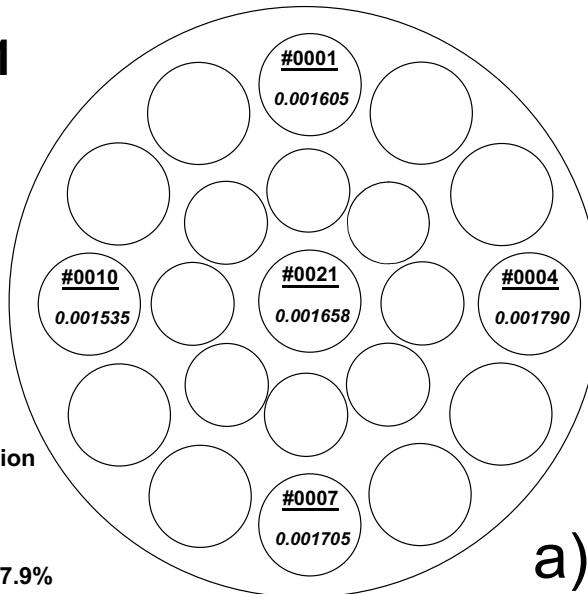
Finally, to derive correction factors for the reactions $^{40}\text{Ca} (n,n\alpha) ^{36}\text{Ar}$, $^{40}\text{Ca} (n,\alpha) ^{37}\text{Ar}$, and $^{42}\text{Ca} (n,\alpha) ^{39}\text{Ar}$ we irradiated grains of natural fluorite which were degassed at ca. 1200°C in the K-Ar extraction line at USP and synthetic Ca-Si-glass. To correct for the reaction $^{40}\text{K} (n,p) ^{40}\text{Ar}$, we irradiated synthetic K_2SO_4 salt grains precipitated from a solution made with analytical grade salts. Total fusion analysis of these grains yielded the correction factors listed in Table I. These values are similar to values for these correction factors obtained from similar reactors elsewhere (McDougall and Harrison 1999). The $(^{39}\text{Ar}/^{37}\text{Ar})\text{Ca}$ correction factor originally obtained from the natural fluorite sample [$15.52(\pm 0.15) \times 10^{-4}$] was higher than the same correction factor obtained from the irradiation of the synthetic Ca-Si-glass [$6.41(\pm 0.04) \times 10^{-4}$] and twice as large as values obtained for other reactors. The higher correction factor obtained from the natural fluorite sample probably indicates trace K contents in the fluorite, and these values have been discarded.

STANDARD ANALYSIS

Irrespective of the quality of instrumentation, environmental conditions, or analytical procedures implemented in a laboratory, the only reliable test of the accuracy and precision of geochronology results is the routine analysis of international standards. To this end, we irradiated and analyzed the standards listed in Table II, obtaining the results shown in Tables II and III, and illustrated below. The standards were irradiated and analyzed as unknowns using Fish Canyon sanidine (Berkeley split # 2, 590-710 μm size range), irradiated in the geometry shown in Fig. 17, as the neutron fluence monitor. All standards, except for P-207 and JTS-1 muscovite and two crystals of GA 1550 biotite, were

SPA9901 without rotation Position

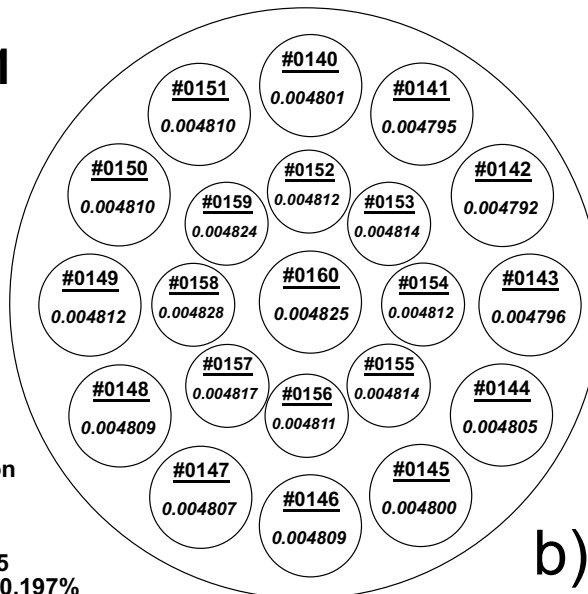
J for Disk:
24.6-hour irradiation
Max 0.001790
Min 0.001535
Mean = 0.001635
Stdev = 0.00013
Coef. Variation = 7.9%



a)

SPA0001 with rotation Position 58-5

J for Disk:
30-hour irradiation
Max 0.004828
Min 0.004792
Mean = 0.00481
Stdev = 0.0000095
Coef. Variation = 0.197%



b)

Fig. 19 – The numbers in each irradiation disk well (a and b) illustrate the J factors obtained through the irradiation of Fish Canyon sanidine neutron fluence monitors. The disk in (a) was irradiated in a stationary position, yielding a 7.9% coefficient of variation for the J factor, revealing the large horizontal heterogeneity in the neutron flux. These results indicate that sample irradiation in a stationary position is unsuitable for $^{40}\text{Ar}/^{39}\text{Ar}$ geochronology unless samples and standards are placed in the same well. This solution, although possible, would require the analysis of neutron fluence monitors for each sample analyzed, decreasing dramatically the productivity of the laboratory. Figure 19b illustrates the extremely homogeneous distribution in J-factors (coefficient of variation = 0.197%) obtained when a disk of Fish Canyon sanidine neutron fluence monitors is irradiated in a rotatable Al-rod. The rotational and precessional movement of the disk during irradiation ensures that each pit position receives approximately the same neutron dosage, compensating for the heterogeneity in the neutron flux.

Irradiation SPA0001 J Factors at each position in irradiation ampoule

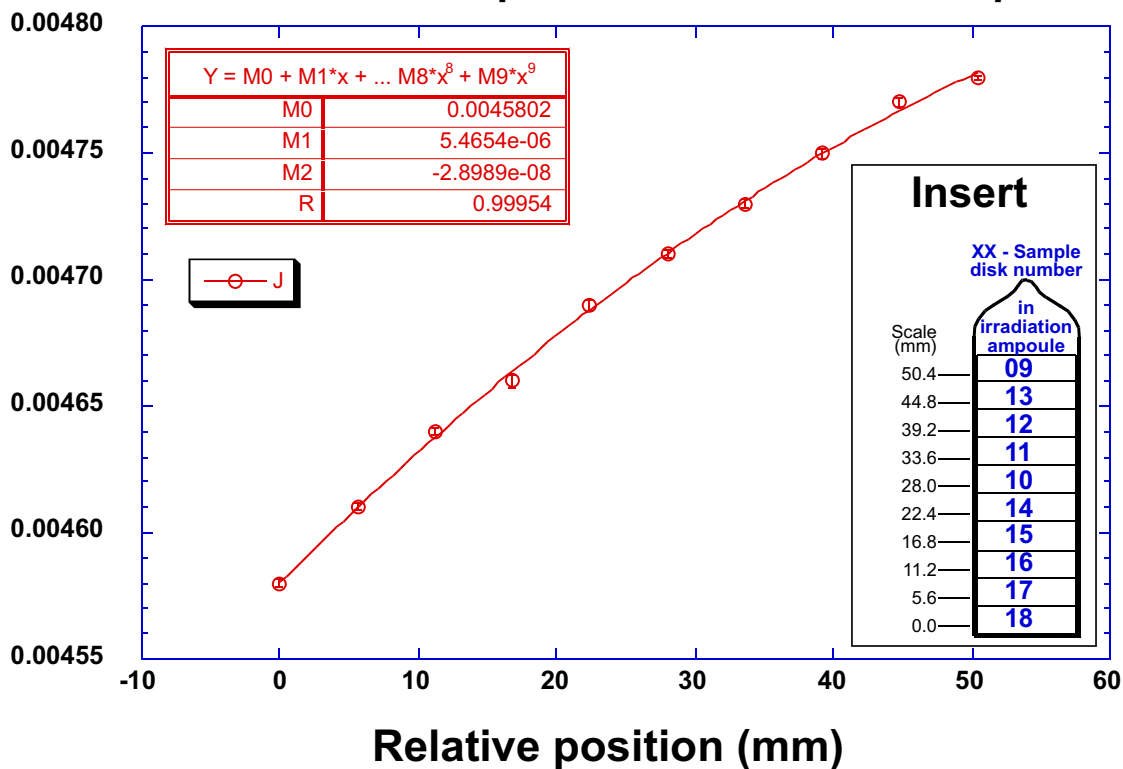


Fig. 20 – Fish Canyon sanidine neutron fluence monitors positioned in a cross pattern in the irradiation disks as illustrated in Fig. 17 were irradiated and analyzed for each of the 10 stacked disks illustrated in the insert. The J factors measured illustrate the vertical heterogeneity in the neutron flux.

TABLE I

Data on the IPEN-USP nuclear reactor used for irradiation by the CP-Geo Ar Laboratory.

Reactor, location, and irradiation position	Type	Cadmium Shielding	Slow Neutron flux (n.cm ⁻² .s ⁻¹) (×10 ¹³)	Epithermal Neutron flux (n.cm ⁻² .s ⁻¹) (×10 ¹³)	Fast Neutron flux (n.cm ⁻² .s ⁻¹) (×10 ¹³)
IPEN IEA-R1 USP, São Paulo, Brazil EIF (58-Level 5)	swimming pool swimming pool	1.5 mm Cd	4.72	2.91	1.68
Reactor, location, and irradiation position	J/h (×10 ⁻⁴)	^{(36)Ar/^{(37)Ar}Ca (×10⁻⁴)}	^{(39)Ar/^{(37)Ar}Ca (×10⁻⁴)}	^{(40)Ar/^{(39)Ar}K (×10⁻⁴)}	
IPEN IEA-R1 USP, São Paulo, Brazil EIF (58-Level 5)	1.6	2.39 ± 0.01	6.41 ± 0.04	7.7 ± 2	

analyzed by the laser total fusion method. It is worth noting that during the analysis of all standards (except P-207, two grains from GA 1550, and JTS-1) a poor connection between the high voltage supply and the emission regulator in the mass spectrometer (since then fixed) introduced undesirable noise in the system, lowering the quality of the analytical results. Despite these technical difficulties, we will show below that the results obtained for the international standards analyzed are indistinguishable, at the 2σ level, from the accepted age values for these standards.

ALDER CREEK SANIDINE

Fourty grains of Alder Creek sanidine (10–20 mesh) were irradiated as shown in Fig. 21c (insert) and analyzed by the total fusion method. Laser-mineral interaction was ensured through the use of zero age glasses placed in the same sample wells as the irradiated grains. One grain failed to interact with the laser and yielded no results. The results for the other grains, separated into two distinct populations due to differences in irradiation positions (Fig. 21c insert), are illustrated in Fig. 21 and listed in Table II. Two grains yield distinctively different results (1.34 and 1.26 Ma, respectively) from the other 37 grains analyzed. It is unclear at this stage whether these outliers indicate heterogeneity in the sample population. The diagrams and the tabulated results show that the measured age for this standard (1.189 ± 0.005 Ma) is indistinguishable, at the 2σ confidence level, from the proposed values for this standard (1.186 ± 0.006 , Turrin et al. 1994; 1.194 ± 0.007 Ma, Renne et al. 1998).

BERN 4M (MUSCOVITE) & BERN 4B (BIOTITE)

Nine grains of Bern 4M and 6 grains of Bern 4B (10–20 mesh) were irradiated and analyzed by the total fusion method. The total fusion results, plotted as $\%^{39}\text{Ar}$ released vs. apparent age in Fig. 22a, show that the apparent ages are not reproducible at 1σ level; however, the results cluster around the accepted K-Ar values for these standards (Table III). Probability density plots for the grains analyzed

(Fig. 22b), at the 1σ level, yield weighted mean ages of 17.3 ± 0.3 Ma for Bern4B and 18.53 ± 0.17 Ma for Bern 4M, results indistinguishable, at the 2σ confidence interval, from the accepted values for these standards (Table III). It is not possible, at this stage, to ascertain whether the spread of the results reflects true heterogeneity in the grains analyzed or whether it reflects noise in the instrumentation, as discussed above.

PALA KA-86 (LEPIDOLITE) & PALA KA-83 (K-FELDSPAR)

Ten grains of KA-86 and 9 grains of KA-83 (10–20 mesh) were irradiated and analyzed by the total fusion method. The results, also plotted as $\%^{39}\text{Ar}$ released vs. apparent age in Fig. 23a, show that the apparent ages obtained are again not reproducible at 1σ level. Probability density plots for the grains analyzed (Fig. 23b) yield weighted mean ages of 92.6 ± 0.5 Ma for KA-83 and 97.9 ± 0.3 Ma for KA-86, results indistinguishable, at the 2σ confidence interval, from the accepted values for these standards (Table III). Again, it is not possible at this stage to ascertain whether the spread of the results reflects true heterogeneity in the grains analyzed or whether it reflects analytical uncertainties.

GA-1550 BIOTITE

Twenty-four single crystals or fragments of crystals of GA 1550 biotite, irradiated in two different disks, were analyzed by the total fusion methods. The results (listed in Table III and illustrated in Fig. 24a and b) reveal a relatively homogenous age distribution, with a mean weighted value for all the grains analyzed of 99.08 ± 0.15 Ma. This value is indistinguishable for the proposed value, 98.8 ± 0.5 Ma, for this standard (Renne et al. 1998). Two single crystals were also analyzed by the incremental-heating method (Fig. 24c and d), yielding plateau ages of 98.0 ± 0.3 and 97.3 ± 0.3 Ma (each step displays 2σ errors and plateau ages are defined as three or more contiguous steps whose uncertainty are within 2σ from the mean), results also compatible with the proposed age for these standards.

TABLE II
 $^{40}\text{Ar}/^{39}\text{Ar}$ results for standards.

Run ID#	Sample	Mixtral	$^{40}\text{Ar}/^{39}\text{Ar}$	$^{38}\text{Ar}/^{39}\text{Ar}$	$^{37}\text{Ar}/^{39}\text{Ar}$	$^{36}\text{Ar}/^{39}\text{Ar}$	$^{40}\text{Ar}/^{39}\text{Ar}$	% Rad.	ΔAge	\pm	Irрад.	J	\pm	^{40}Ar	^{40}Ar
									(Ma)	(Ma)				(nA)	(moles)
228-01	AC	sunshine	0.1551	1.104E-02	9.651E-03	4.481E-05	0.1419	91.9	1.220	0.006	SPA0001-13	0.00477	1.69E-06	0.4659	8.916E-15
228-03	AC	sunshine	0.1471	1.065E-02	8.462E-03	2.895E-05	0.1385	94.6	1.191	0.009	SPA0001-13	0.00477	1.69E-06	0.4457	8.470E-15
228-04	AC	sunshine	0.1413	1.079E-02	9.008E-03	7.753E-06	0.1389	98.8	1.195	0.010	SPA0001-13	0.00477	1.69E-06	0.3066	5.844E-15
228-05	AC	sunshine	0.1393	1.074E-02	9.131E-03	1.535E-05	0.1347	97.2	1.159	0.006	SPA0001-13	0.00477	1.69E-06	0.3433	6.551E-15
228-06	AC	sunshine	0.1447	1.084E-02	8.784E-03	2.977E-05	0.1338	94.3	1.168	0.005	SPA0001-13	0.00477	1.69E-06	0.7237	1.383E-14
228-07	AC	sunshine	0.1429	1.085E-02	9.941E-03	1.942E-05	0.1372	96.5	1.180	0.006	SPA0001-13	0.00477	1.69E-06	0.4083	7.806E-15
228-08	AC	sunshine	0.1421	1.082E-02	8.899E-03	1.559E-05	0.1375	97.2	1.183	0.006	SPA0001-13	0.00477	1.69E-06	0.4270	8.136E-15
228-09	AC	sunshine	0.1419	1.079E-02	9.915E-03	1.946E-05	0.1362	96.4	1.171	0.005	SPA0001-13	0.00477	1.69E-06	0.5310	1.015E-14
228-10	AC	sunshine	0.1436	1.084E-02	8.974E-03	2.998E-05	0.1347	94.2	1.158	0.007	SPA0001-13	0.00477	1.69E-06	0.2920	5.575E-15
228-11	AC	sunshine	0.1430	1.088E-02	8.717E-03	1.624E-05	0.1381	97.0	1.188	0.006	SPA0001-13	0.00477	1.69E-06	0.3471	6.625E-15
228-12	AC	sunshine	0.1443	1.084E-02	9.974E-03	2.881E-05	0.1338	94.6	1.168	0.005	SPA0001-13	0.00477	1.69E-06	0.5402	1.028E-14
228-13	AC	sunshine	0.1439	1.088E-02	1.064E-02	1.503E-05	0.1395	97.4	1.200	0.008	SPA0001-13	0.00477	1.69E-06	0.2840	5.411E-15
228-14	AC	sunshine	0.1422	1.075E-02	1.008E-02	1.826E-05	0.1369	96.7	1.177	0.006	SPA0001-13	0.00477	1.69E-06	0.3153	5.999E-15
228-15	AC	sunshine	0.1408	1.075E-02	9.781E-03	1.406E-05	0.1367	97.5	1.176	0.008	SPA0001-13	0.00477	1.69E-06	0.2867	5.465E-15
228-16	AC	sunshine	0.1448	1.072E-02	9.062E-03	2.985E-05	0.1359	94.3	1.169	0.005	SPA0001-13	0.00477	1.69E-06	0.4992	9.511E-15
228-17	AC	sunshine	0.1446	1.074E-02	9.142E-03	2.586E-05	0.1369	95.1	1.178	0.005	SPA0001-13	0.00477	1.69E-06	0.4911	9.349E-15
228-18	AC	sunshine	0.1404	1.082E-02	8.738E-03	1.288E-05	0.1367	97.9	1.176	0.004	SPA0001-13	0.00477	1.69E-06	0.6021	1.158E-14
228-19	AC	sunshine	0.1411	1.079E-02	9.053E-03	2.044E-06	0.1404	100.0	1.208	0.018	SPA0001-13	0.00477	1.69E-06	0.0858	1.633E-15
228-20	AC	sunshine	0.1420	1.077E-02	1.085E-02	-2.120E-06	0.1427	101.0	1.228	0.013	SPA0001-13	0.00477	1.69E-06	0.1259	2.397E-15
234-01	AC	sunshine	0.1437	1.055E-02	8.571E-03	1.688E-05	0.1386	96.9	1.193	0.007	SPA0001-13	0.00477	1.69E-06	0.3213	6.112E-15
234-02	AC	sunshine	0.1434	1.103E-02	9.492E-03	2.536E-05	0.1364	95.6	1.173	0.006	SPA0001-13	0.00477	1.69E-06	0.3329	6.348E-15
234-03	AC	sunshine	0.1432	1.069E-02	8.775E-03	1.909E-05	0.1375	96.5	1.183	0.006	SPA0001-13	0.00477	1.69E-06	0.4287	8.187E-15
234-04	AC	sunshine	0.1448	1.075E-02	8.303E-03	1.518E-05	0.1402	97.3	1.205	0.011	SPA0001-13	0.00477	1.69E-06	0.1966	3.738E-15
234-05	AC	sunshine	0.1488	1.075E-02	8.945E-03	3.142E-05	0.1394	94.2	1.200	0.005	SPA0001-13	0.00477	1.69E-06	0.5311	1.011E-14
234-06	AC	sunshine	0.1480	1.082E-02	1.075E-02	4.143E-05	0.1338	92.2	1.168	0.006	SPA0001-13	0.00477	1.69E-06	0.4927	9.397E-15
234-07	AC	sunshine	0.1430	1.082E-02	1.062E-02	1.905E-05	0.1374	96.6	1.182	0.006	SPA0001-13	0.00477	1.69E-06	0.4278	8.121E-15
234-08	AC	sunshine	0.1591	1.075E-02	8.841E-03	6.366E-05	0.1402	88.5	1.205	0.006	SPA0001-13	0.00477	1.69E-06	0.5502	1.048E-14
234-09	AC	sunshine	0.1610	1.071E-02	1.375E-02	1.944E-05	0.1555	97.0	1.338	0.007	SPA0001-13	0.00477	1.69E-06	0.3423	6.528E-15
234-10	AC	sunshine	0.1450	1.088E-02	8.968E-03	2.794E-05	0.1367	94.7	1.176	0.010	SPA0001-13	0.00477	1.69E-06	0.1874	3.573E-15
234-11	AC	sunshine	0.1429	1.074E-02	9.404E-03	1.533E-05	0.1383	97.3	1.190	0.005	SPA0001-13	0.00477	1.69E-06	0.4872	9.271E-15
234-12	AC	sunshine	0.1520	1.054E-02	9.838E-03	4.138E-05	0.1398	92.4	1.202	0.007	SPA0001-13	0.00477	1.69E-06	0.3921	7.455E-15
234-13	AC	sunshine	0.1501	1.078E-02	1.371E-02	1.205E-05	0.1468	98.3	1.263	0.005	SPA0001-13	0.00477	1.69E-06	0.4046	7.727E-15
234-14	AC	sunshine	0.1481	1.058E-02	8.863E-03	3.857E-05	0.1366	92.7	1.175	0.008	SPA0001-13	0.00477	1.69E-06	0.3316	6.334E-15
234-15	AC	sunshine	0.1426	1.087E-02	9.256E-03	7.151E-06	0.1404	99.0	1.208	0.007	SPA0001-13	0.00477	1.69E-06	0.2398	4.560E-15
234-16	AC	sunshine	0.1409	1.088E-02	9.212E-03	9.700E-06	0.1380	98.4	1.187	0.007	SPA0001-13	0.00477	1.69E-06	0.3104	5.942E-15
234-17	AC	sunshine	0.1424	1.073E-02	1.040E-02	1.868E-05	0.1369	96.6	1.178	0.006	SPA0001-13	0.00477	1.69E-06	0.3937	7.538E-15
234-18	AC	sunshine	0.1474	1.086E-02	9.049E-03	3.406E-05	0.1373	93.6	1.181	0.006	SPA0001-13	0.00477	1.69E-06	0.3606	6.883E-15
234-19	AC	sunshine	0.1521	1.088E-02	8.840E-03	4.398E-05	0.1390	91.8	1.196	0.010	SPA0001-13	0.00477	1.69E-06	0.2110	4.023E-15
234-20	AC	sunshine	0.1424	1.073E-02	1.037E-02	1.730E-05	0.1373	96.9	1.181	0.007	SPA0001-13	0.00477	1.69E-06	0.3184	6.097E-15

arithmetic mean = 1.192 0.007
sdev = 0.031
median = 1.183 0.006
weighted mean \pm error = 1.189 \pm 0.005 Ma

TABLE II (continuation)

Run ID#	Sample	Mineral	$^{40}\text{Ar}/^{39}\text{Ar}$	$^{38}\text{Ar}/^{39}\text{Ar}$	$^{37}\text{Ar}/^{39}\text{Ar}$	$^{36}\text{Ar}/^{39}\text{Ar}$	$^{40}\text{Ar}^*/^{39}\text{Ar}$	% Rad	Age (Ma)	± (Ma)	Irrad.	J	±	^{40}Ar (nA)	^{40}Ar (moles)
304-02	GA-1550	biotite	11,681	1,56E-02	0,00E+00	-1,66E-03	12,17	104,2	99,12	0,70	SPA0001-16	0,00464	1,57E-06	0,811	1,55E-14
304-03	GA-1550	biotite	12,859	1,62E-02	0,00E+00	2,26E-03	12,19	94,8	99,27	0,95	SPA0001-16	0,00464	1,57E-06	0,686	1,39E-14
304-04	GA-1550	biotite	12,906	1,69E-02	0,00E+00	2,50E-03	12,17	94,3	99,08	0,66	SPA0001-16	0,00464	1,57E-06	0,503	9,63E-15
304-05	GA-1550	biotite	12,919	1,77E-02	5,74E-03	2,94E-03	12,05	93,3	98,16	0,38	SPA0001-16	0,00464	1,57E-06	0,602	1,15E-14
304-06	GA-1550	biotite	13,297	1,56E-02	2,10E-02	3,53E-03	12,25	92,2	99,77	0,40	SPA0001-16	0,00464	1,57E-06	0,676	1,30E-14
304-07	GA-1550	biotite	12,851	1,65E-02	0,00E+00	1,63E-03	12,37	96,3	100,68	0,67	SPA0001-16	0,00464	1,57E-06	0,425	8,13E-15
304-08	GA-1550	biotite	12,707	1,48E-02	0,00E+00	1,54E-03	12,25	96,4	99,75	0,41	SPA0001-16	0,00464	1,57E-06	0,619	1,20E-14
304-09	GA-1550	biotite	13,093	1,18E-02	3,23E-03	3,08E-03	12,18	93,0	99,19	0,81	SPA0001-16	0,00464	1,57E-06	1,335	2,72E-14
304-10	GA-1550	biotite	13,130	1,63E-02	0,00E+00	2,87E-03	12,28	93,5	99,99	0,33	SPA0001-16	0,00464	1,57E-06	0,527	1,01E-14
304-11	GA-1550	biotite	12,479	1,71E-02	1,52E-02	1,52E-03	12,03	96,4	97,98	0,25	SPA0001-16	0,00464	1,57E-06	1,495	2,85E-14
304-12	GA-1550	biotite	12,573	1,68E-02	0,00E+00	1,51E-03	12,13	96,5	98,75	0,23	SPA0001-16	0,00464	1,57E-06	1,828	3,49E-14
315-01	GA-1550	biotite	14,058	1,79E-02	2,99E-03	5,97E-03	12,29	87,5	99,45	0,34	SPA0001-17	0,00461	1,54E-06	1,264	2,49E-14
315-02	GA-1550	biotite	12,575	1,73E-02	0,00E+00	1,33E-03	12,18	96,9	98,56	0,44	SPA0001-17	0,00461	1,54E-06	0,651	1,25E-14
315-03	GA-1550	biotite	12,491	1,60E-02	3,68E-03	1,24E-03	12,13	97,1	98,13	0,37	SPA0001-17	0,00461	1,54E-06	0,678	1,29E-14
315-04	GA-1550	biotite	13,221	1,60E-02	3,27E-03	3,20E-03	12,28	92,9	99,32	0,42	SPA0001-17	0,00461	1,54E-06	0,583	1,11E-14
315-05	GA-1550	biotite	12,925	1,57E-02	0,00E+00	2,07E-03	12,31	95,3	99,59	0,30	SPA0001-17	0,00461	1,54E-06	0,809	1,55E-14
315-06	GA-1550	biotite	12,696	1,59E-02	1,90E-03	1,39E-03	12,28	96,8	99,38	0,33	SPA0001-17	0,00461	1,54E-06	0,867	1,66E-14
315-07	GA-1550	biotite	13,425	1,82E-02	0,00E+00	4,16E-03	12,20	90,8	98,68	0,73	SPA0001-17	0,00461	1,54E-06	0,463	8,71E-15
315-08	GA-1550	biotite	13,443	1,51E-02	0,00E+00	4,09E-03	12,23	91,0	98,98	0,45	SPA0001-17	0,00461	1,54E-06	0,572	1,09E-14
315-09	GA-1550	biotite	14,049	1,67E-02	0,00E+00	5,98E-03	12,28	87,4	99,35	0,28	SPA0001-17	0,00461	1,54E-06	1,205	2,30E-14
315-10	GA-1550	biotite	12,634	1,53E-02	0,00E+00	1,11E-03	12,31	97,4	99,54	0,36	SPA0001-17	0,00461	1,54E-06	0,640	1,22E-14
315-11	GA-1550	biotite	13,034	1,57E-02	0,00E+00	2,58E-03	12,27	94,1	99,26	0,44	SPA0001-17	0,00461	1,54E-06	0,569	1,09E-14
315-12	GA-1550	biotite	13,004	1,73E-02	2,05E-03	2,54E-03	12,25	94,2	99,13	0,33	SPA0001-17	0,00461	1,54E-06	0,898	1,72E-14
315-13	GA-1550	biotite	13,043	1,70E-02	3,79E-03	2,68E-03	12,25	93,9	99,11	0,30	SPA0001-17	0,00461	1,54E-06	1,044	1,99E-14
arithmetic mean = 99,17 0,45															
stdev = 0,61															
median = 99,22 0,39															
weighted mean ± error = 99,08 ± 0,15 Ma															

TABLE II (continuation)

Run ID#	Sample	Mineral	$^{40}\text{Ar}/^{39}\text{Ar}$	$^{38}\text{Ar}/^{39}\text{Ar}$	$^{37}\text{Ar}/^{39}\text{Ar}$	$^{36}\text{Ar}/^{39}\text{Ar}$	$^{40}\text{Ar} * /^{39}\text{Ar}$	% Rad	Age	±	Irrad.	J	±	^{40}Ar	^{40}Ar
									(Ma)	(Ma)				(nA)	(moles)
194-02	BERN-4M	muscovite	3,067	1,13E-02	8,90E-04	2,83E-03	2,229	72,7	18,92	0,23	SPA0001-11	0,00473	1,58E-06	0,360	6,88E-15
194-03	BERN-4M	muscovite	2,820	1,14E-02	0,00E+00	2,03E-03	2,219	78,7	18,84	0,12	SPA0001-11	0,00473	1,58E-06	0,522	9,98E-15
194-04	BERN-4M	muscovite	3,372	1,12E-02	2,35E-03	3,74E-03	2,265	67,2	19,23	0,35	SPA0001-11	0,00473	1,58E-06	0,332	6,29E-15
194-05	BERN-4M	muscovite	3,839	1,14E-02	4,03E-04	5,34E-03	2,261	58,9	19,19	0,19	SPA0001-11	0,00473	1,58E-06	0,543	1,04E-14
194-06	BERN-4M	muscovite	2,467	1,06E-02	0,00E+00	1,23E-03	2,104	85,3	17,87	0,13	SPA0001-11	0,00473	1,58E-06	0,351	6,77E-15
194-07	BERN-4M	muscovite	4,112	1,17E-02	3,69E-04	6,67E-03	2,142	52,1	18,18	0,29	SPA0001-11	0,00473	1,58E-06	0,506	9,80E-15
194-08	BERN-4M	muscovite	3,121	1,09E-02	0,00E+00	3,10E-03	2,202	70,6	18,70	0,22	SPA0001-11	0,00473	1,58E-06	0,389	7,42E-15
194-09	BERN-4M	muscovite	3,041	1,10E-02	3,72E-03	2,95E-03	2,169	71,3	18,41	0,28	SPA0001-11	0,00473	1,58E-06	0,680	1,30E-14
194-10	BERN-4M	muscovite	2,959	1,11E-02	1,12E-05	2,72E-03	2,154	72,8	18,29	0,14	SPA0001-11	0,00473	1,58E-06	0,474	9,04E-15
arithmetic mean = 18,63 0,22															
stdev = 0,47															
median = 18,70 0,22															
weighted mean ± error = 18.53 ± 0.17 Ma															
172-02	BERN-4B	biotite	2,297	1,07E-02	8,01E-03	8,83E-04	2,036	88,7	17,22	0,16	SPA0001-10	0,00471	1,59E-06	0,176	3,36E-15
172-04	BERN-4B	biotite	2,442	1,07E-02	0,00E+00	9,25E-04	2,168	88,8	18,33	0,23	SPA0001-10	0,00471	1,59E-06	0,153	2,91E-15
172-05	BERN-4B	biotite	2,346	1,06E-02	0,00E+00	9,01E-04	2,079	88,6	17,58	0,25	SPA0001-10	0,00471	1,59E-06	0,114	2,16E-15
172-06	BERN-4B	biotite	2,566	1,13E-02	0,00E+00	1,58E-03	2,097	81,7	17,73	0,30	SPA0001-10	0,00471	1,59E-06	0,085	1,62E-15
172-07	BERN-4B	biotite	2,384	1,13E-02	9,63E-03	1,21E-03	2,026	85,0	17,14	0,23	SPA0001-10	0,00471	1,59E-06	0,116	2,22E-15
172-10	BERN-4B	biotite	2,268	1,06E-02	0,00E+00	9,40E-04	1,990	87,8	16,83	0,16	SPA0001-10	0,00471	1,59E-06	0,217	4,10E-15
172-09A	BERN-4B	biotite	2,611	1,07E-02	0,00E+00	9,52E-04	2,329	89,2	19,68	1,27	SPA0001-10	0,00471	1,59E-06	0,022	4,26E-16
arithmetic mean = 17,79 0,22															
stdev = 0,96															
median = 17,58 0,23															
weighted mean ± error = 17.3 ± 0.2 Ma															

TABLE II (continuation)

Run ID#	Sample	Mineral	$^{40}\text{Ar}/^{39}\text{Ar}$	$^{38}\text{Ar}/^{39}\text{Ar}$	$^{37}\text{Ar}/^{39}\text{Ar}$	$^{36}\text{Ar}/^{39}\text{Ar}$	$^{40}\text{Ar}^*/^{39}\text{Ar}$	% Rad	Age (Ma)	± (Ma)	Irrad.	J	±	^{40}Ar (nA)	^{40}Ar (moles)
183-01	KA-86	lepidolite	12,410	1,12E-02	0,00E+00	1,96E-03	11,832	95,3	98,24	0,25	SPA0001-11	0,00473	1,58E-06	13,449	2,57E-13
183-02	KA-86	lepidolite	12,301	1,11E-02	0,00E+00	1,91E-03	11,737	95,4	97,47	0,19	SPA0001-11	0,00473	1,58E-06	15,132	2,89E-13
183-03	KA-86	lepidolite	12,116	1,11E-02	0,00E+00	9,33E-04	11,840	97,7	98,30	0,37	SPA0001-11	0,00473	1,58E-06	11,394	2,17E-13
183-04	KA-86	lepidolite	12,692	1,14E-02	0,00E+00	2,74E-03	11,880	93,6	98,63	0,42	SPA0001-11	0,00473	1,58E-06	10,165	1,94E-13
183-05	KA-86	lepidolite	12,162	1,11E-02	0,00E+00	1,27E-03	11,786	96,9	97,87	0,26	SPA0001-11	0,00473	1,58E-06	18,894	3,65E-13
183-06	KA-86	lepidolite	12,570	1,12E-02	1,33E-03	2,73E-03	11,762	93,6	97,67	0,25	SPA0001-11	0,00473	1,58E-06	3,230	6,17E-14
183-07	KA-86	lepidolite	12,168	1,10E-02	0,00E+00	1,46E-03	11,735	96,4	97,46	0,23	SPA0001-11	0,00473	1,58E-06	5,702	1,09E-13
183-08	KA-86	lepidolite	12,910	1,15E-02	0,00E+00	3,14E-03	11,983	92,8	99,46	0,62	SPA0001-11	0,00473	1,58E-06	11,059	2,15E-13
183-09	KA-86	lepidolite	12,515	1,13E-02	0,00E+00	2,45E-03	11,791	94,2	97,91	0,26	SPA0001-11	0,00473	1,58E-06	13,926	2,66E-13
183-10	KA-86	lepidolite	12,655	1,14E-02	0,00E+00	2,84E-03	11,817	93,4	98,12	0,28	SPA0001-11	0,00473	1,58E-06	1,733	3,32E-14
arithmetic mean = 98,11 0,31															
stdev = 0,60															
median = 98,01 0,26															
weighted mean ± error = 97,9 ± 0,3 Ma															
187-01	KA-83	orthoclase	11,692	1,10E-02	0,00E+00	1,74E-03	11,177	95,6	92,94	0,25	SPA0001-11	0,00473	1,58E-06	28,935	5,55E-13
187-02	KA-83	orthoclase	11,752	1,10E-02	0,00E+00	2,05E-03	11,145	94,8	92,68	0,22	SPA0001-11	0,00473	1,58E-06	16,932	3,25E-13
187-03	KA-83	orthoclase	11,690	1,10E-02	0,00E+00	1,43E-03	11,268	96,4	93,67	0,44	SPA0001-11	0,00473	1,58E-06	21,477	4,17E-13
187-04	KA-83	orthoclase	14,322	1,28E-02	0,00E+00	1,09E-02	11,112	77,6	92,41	0,50	SPA0001-11	0,00473	1,58E-06	25,838	5,00E-13
187-05	KA-83	orthoclase	11,784	1,09E-02	0,00E+00	2,51E-03	11,041	93,7	91,84	0,45	SPA0001-11	0,00473	1,58E-06	32,994	6,29E-13
187-06	KA-83	orthoclase	12,159	1,13E-02	0,00E+00	3,15E-03	11,226	92,3	93,34	0,22	SPA0001-11	0,00473	1,58E-06	56,626	1,08E-12
187-07	KA-83	orthoclase	12,088	1,13E-02	0,00E+00	3,33E-03	11,102	91,8	92,33	0,19	SPA0001-11	0,00473	1,58E-06	21,943	4,19E-13
187-08	KA-83	orthoclase	11,630	1,10E-02	0,00E+00	1,58E-03	11,163	96,0	92,83	0,28	SPA0001-11	0,00473	1,58E-06	43,322	8,28E-13
187-09	KA-83	orthoclase	11,851	1,13E-02	0,00E+00	2,95E-03	10,980	92,7	91,34	0,23	SPA0001-11	0,00473	1,58E-06	14,512	2,78E-13
arithmetic mean = 92,60 0,31															
stdev = 0,72															
median = 92,68 0,25															
weighted mean ± error = 92,6 ± 0,5 Ma															

TABLE II (continuation)

Run ID#	Sample	Mineral	$^{40}\text{Ar}/^{39}\text{Ar}$	$^{38}\text{Ar}/^{39}\text{Ar}$	$^{37}\text{Ar}/^{39}\text{Ar}$	$^{36}\text{Ar}/^{39}\text{Ar}$	$^{40}\text{Ar}^*/^{39}\text{Ar}$	% Rad	Age	±	Irrad.	J	±	^{40}Ar	^{40}Ar
									(Ma)	(Ma)				(nA)	(moles)
0198-01A	P-205	muscovite	12,23	1,41E-02	0,00E+00	1,59E-02	7,55	61,7	63,26	10,56	SPA0001-11	0,00473	1,58E-06	0,013	2,38E-16
0198-01B	P-205	muscovite	11,71	9,31E-03	0,00E+00	6,23E-03	9,87	84,3	82,28	2,17	SPA0001-11	0,00473	1,58E-06	0,065	1,26E-15
0198-01C	P-205	muscovite	10,35	1,10E-02	0,00E+00	1,44E-03	9,92	95,9	82,76	0,36	SPA0001-11	0,00473	1,58E-06	0,489	9,31E-15
0198-01D	P-205	muscovite	10,28	1,09E-02	0,00E+00	9,65E-04	9,99	97,2	83,33	0,22	SPA0001-11	0,00473	1,58E-06	1,460	2,80E-14
0198-01E	P-205	muscovite	9,75	1,05E-02	0,00E+00	2,27E-04	9,69	99,3	80,81	0,20	SPA0001-11	0,00473	1,58E-06	1,631	3,12E-14
0198-01F	P-205	muscovite	9,69	1,04E-02	1,44E-03	1,98E-04	9,63	99,4	80,35	0,22	SPA0001-11	0,00473	1,58E-06	1,063	2,03E-14
0198-01G	P-205	muscovite	9,85	1,03E-02	1,71E-02	3,86E-04	9,74	98,9	81,22	0,59	SPA0001-11	0,00473	1,58E-06	0,232	4,45E-15
0198-01H	P-205	muscovite	9,85	1,06E-02	9,25E-03	1,42E-04	9,81	99,6	81,79	0,25	SPA0001-11	0,00473	1,58E-06	0,944	1,80E-14
0198-01I	P-205	muscovite	10,03	1,10E-02	2,82E-02	4,18E-04	9,91	98,8	82,64	0,51	SPA0001-11	0,00473	1,58E-06	0,298	5,67E-15
0198-02A	P-205	muscovite	11,74	1,31E-02	0,00E+00	1,22E-02	8,14	69,3	68,18	2,54	SPA0001-11	0,00473	1,58E-06	0,058	1,11E-15
0198-02B	P-205	muscovite	10,51	1,11E-02	0,00E+00	2,13E-03	9,88	94	82,41	0,76	SPA0001-11	0,00473	1,58E-06	0,198	3,77E-15
0198-02C	P-205	muscovite	10,27	1,07E-02	0,00E+00	5,70E-04	10,10	98,4	84,17	0,22	SPA0001-11	0,00473	1,58E-06	1,162	2,21E-14
0198-02D	P-205	muscovite	9,96	1,10E-02	1,23E-03	2,57E-04	9,89	99,2	82,46	0,23	SPA0001-11	0,00473	1,58E-06	0,994	1,90E-14
0198-02E	P-205	muscovite	10,03	1,10E-02	1,23E-02	5,03E-04	9,88	98,5	82,42	0,30	SPA0001-11	0,00473	1,58E-06	0,587	1,12E-14
0198-02F	P-205	muscovite	9,98	1,06E-02	0,00E+00	1,95E-04	9,92	99,4	82,71	0,40	SPA0001-11	0,00473	1,58E-06	0,374	7,15E-15
0198-02G	P-205	muscovite	10,09	9,50E-03	0,00E+00	-6,36E-04	10,27	101,9	85,60	0,91	SPA0001-11	0,00473	1,58E-06	0,128	2,44E-15
0198-02H	P-205	muscovite	10,07	1,02E-02	1,06E-02	9,32E-07	10,07	100	83,91	1,16	SPA0001-11	0,00473	1,58E-06	0,111	2,12E-15
0198-02I	P-205	muscovite	10,07	1,05E-02	1,74E-02	5,17E-05	10,05	99,9	83,81	0,46	SPA0001-11	0,00473	1,58E-06	0,327	6,23E-15
0198-02J	P-205	muscovite	10,04	1,04E-02	0,00E+00	-6,47E-04	10,23	101,9	85,26	1,47	SPA0001-11	0,00473	1,58E-06	0,076	1,45E-15
0198-03A	P-205	muscovite	10,15	1,37E-02	1,86E-01	1,00E-02	7,20	70,9	60,41	5,64	SPA0001-11	0,00473	1,58E-06	0,019	3,69E-16
0198-03B	P-205	muscovite	23,17	1,88E-02	2,49E-02	4,86E-02	8,81	38	73,65	3,41	SPA0001-11	0,00473	1,58E-06	0,140	2,68E-15
0198-03C	P-205	muscovite	14,10	1,38E-02	0,00E+00	1,20E-02	10,55	74,8	87,84	1,09	SPA0001-11	0,00473	1,58E-06	0,228	4,35E-15
0198-03D	P-205	muscovite	10,58	1,11E-02	1,96E-03	2,79E-04	10,49	99,2	87,40	0,31	SPA0001-11	0,00473	1,58E-06	0,825	1,58E-14
0198-03E	P-205	muscovite	9,88	1,10E-02	0,00E+00	1,27E-04	9,84	99,6	82,10	0,21	SPA0001-11	0,00473	1,58E-06	1,466	2,81E-14

TABLE II (continuation)

Run ID#	Sample	Mineral	$^{40}\text{Ar}/^{39}\text{Ar}$	$^{38}\text{Ar}/^{39}\text{Ar}$	$^{37}\text{Ar}/^{39}\text{Ar}$	$^{36}\text{Ar}/^{39}\text{Ar}$	$^{40}\text{Ar}^*/^{39}\text{Ar}$	% Rad	Age (Ma)	\pm (Ma)	Irrad.	J	\pm	^{40}Ar (nA)	^{40}Ar (moles)
0198-03F	P-205	muscovite	9,55	1,08E-02	0,00E+00	7,12E-05	9,53	99,8	79,54	0,27	SPA0001-11	0,00473	1,58E-06	0,652	1,24E-14
0198-03G	P-205	muscovite	9,85	1,09E-02	0,00E+00	3,26E-04	9,75	99	81,33	0,25	SPA0001-11	0,00473	1,58E-06	0,836	1,60E-14
0198-03H	P-205	muscovite	9,87	1,06E-02	0,00E+00	3,83E-04	9,75	98,9	81,35	0,48	SPA0001-11	0,00473	1,58E-06	0,294	5,66E-15
0198-03I	P-205	muscovite	9,93	1,09E-02	5,94E-04	2,49E-04	9,86	99,3	82,23	0,27	SPA0001-11	0,00473	1,58E-06	0,658	1,26E-14
0198-03J	P-205	muscovite	9,95	1,09E-02	7,41E-03	1,19E-04	9,92	99,7	82,69	0,30	SPA0001-11	0,00473	1,58E-06	0,589	1,13E-14
0198-04A	P-205	muscovite	10,64	1,13E-02	0,00E+00	9,70E-03	7,77	73	65,10	2,20	SPA0001-11	0,00473	1,58E-06	0,057	1,10E-15
0198-04B	P-205	muscovite	11,24	1,17E-02	1,28E-02	3,72E-03	10,15	90,2	84,57	0,54	SPA0001-11	0,00473	1,58E-06	0,377	7,19E-15
0198-04C	P-205	muscovite	10,15	1,09E-02	2,97E-04	5,93E-04	9,97	98,3	83,16	0,19	SPA0001-11	0,00473	1,58E-06	1,660	3,17E-14
0198-04D	P-205	muscovite	9,73	1,08E-02	0,00E+00	1,94E-04	9,67	99,4	80,67	0,23	SPA0001-11	0,00473	1,58E-06	0,969	1,85E-14
0198-04E	P-205	muscovite	9,68	1,09E-02	0,00E+00	3,79E-04	9,57	98,8	79,87	0,23	SPA0001-11	0,00473	1,58E-06	0,899	1,72E-14
0198-04F	P-205	muscovite	9,66	1,08E-02	3,42E-03	5,10E-04	9,51	98,4	79,35	0,35	SPA0001-11	0,00473	1,58E-06	0,429	8,20E-15
0198-04G	P-205	muscovite	9,60	1,12E-02	6,16E-05	6,26E-04	9,42	98,1	78,61	0,49	SPA0001-11	0,00473	1,58E-06	0,268	5,12E-15
0198-04H	P-205	muscovite	9,50	1,10E-02	0,00E+00	7,34E-04	9,28	97,7	77,50	0,40	SPA0001-11	0,00473	1,58E-06	0,385	7,31E-15
0198-04I	P-205	muscovite	9,87	1,15E-02	8,23E-03	4,45E-04	9,74	98,7	81,24	0,56	SPA0001-11	0,00473	1,58E-06	0,234	4,49E-15
0198-04J	P-205	muscovite	9,86	1,08E-02	1,14E-02	2,11E-04	9,79	99,4	81,70	0,41	SPA0001-11	0,00473	1,58E-06	0,338	6,46E-15
0198-05A	P-205	muscovite	12,75	1,42E-02	0,00E+00	1,51E-02	8,28	64,9	69,32	3,15	SPA0001-11	0,00473	1,58E-06	0,046	8,78E-16
0198-05B	P-205	muscovite	10,40	1,06E-02	0,00E+00	1,54E-03	9,94	95,6	82,88	0,41	SPA0001-11	0,00473	1,58E-06	0,453	8,63E-15
0198-05C	P-205	muscovite	10,01	1,08E-02	3,45E-03	9,39E-04	9,73	97,2	81,18	0,28	SPA0001-11	0,00473	1,58E-06	0,648	1,24E-14
0198-05D	P-205	muscovite	10,13	1,11E-02	0,00E+00	5,68E-04	9,97	98,3	83,10	0,20	SPA0001-11	0,00473	1,58E-06	1,911	3,66E-14
0198-05E	P-205	muscovite	9,82	1,07E-02	0,00E+00	1,21E-04	9,79	99,6	81,63	0,20	SPA0001-11	0,00473	1,58E-06	1,376	2,62E-14
0198-05F	P-205	muscovite	9,76	1,07E-02	0,00E+00	1,56E-04	9,71	99,5	81,02	0,31	SPA0001-11	0,00473	1,58E-06	0,573	1,09E-14
0198-05G	P-205	muscovite	9,83	1,05E-02	0,00E+00	2,54E-04	9,76	99,2	81,41	0,37	SPA0001-11	0,00473	1,58E-06	0,402	7,66E-15
0198-05H	P-205	muscovite	9,88	1,05E-02	0,00E+00	3,15E-04	9,79	99,1	81,66	0,45	SPA0001-11	0,00473	1,58E-06	0,287	5,50E-15
0198-05I	P-205	muscovite	9,97	1,05E-02	0,00E+00	3,35E-05	9,96	99,9	83,04	0,29	SPA0001-11	0,00473	1,58E-06	0,515	9,81E-15
0198-05J	P-205	muscovite	9,91	1,06E-02	0,00E+00	-1,04E-04	9,94	100,3	82,89	0,32	SPA0001-11	0,00473	1,58E-06	0,536	1,03E-14
arithmetic mean = 80,36 0,60															
stdev = 5,72															
median = 81,65 0,31															
weighted mean \pm error = 82,0 \pm 0,5 Ma															

TABLE II (continuation)

Run ID#	Sample	Mineral	40Ar/39Ar	38Ar/39Ar	37Ar/39Ar	36Ar/39Ar	40Ar*/39Ar	% Rad	Age	±	Irrad.	J	±	40Ar	40Ar
									(Ma)	(Ma)				(nA)	(moles)
0184-01A	JTS-1	muscovite	100,32	3,02E-02	0,00E+00	1,07E-01	68,64	68,4	507,26	14,34	SPA0001-11	0,00473	1,58E-06	0,136	2,60E-15
0184-01B	JTS-1	muscovite	77,16	1,49E-02	0,00E+00	9,90E-03	74,23	96,2	542,90	6,20	SPA0001-11	0,00473	1,58E-06	0,256	4,89E-15
0184-01C	JTS-1	muscovite	81,62	1,14E-02	0,00E+00	1,06E-02	78,50	96,2	569,64	4,51	SPA0001-11	0,00473	1,58E-06	0,560	1,07E-14
0184-01D	JTS-1	muscovite	78,21	1,12E-02	0,00E+00	3,16E-03	77,27	98,8	562,01	1,93	SPA0001-11	0,00473	1,58E-06	1,531	2,93E-14
0184-01E	JTS-1	muscovite	78,14	1,09E-02	0,00E+00	2,26E-03	77,47	99,1	563,24	1,30	SPA0001-11	0,00473	1,58E-06	5,664	1,08E-13
0184-01F	JTS-1	muscovite	77,76	1,09E-02	0,00E+00	7,75E-04	77,53	99,7	563,61	1,09	SPA0001-11	0,00473	1,58E-06	12,120	2,33E-13
0184-01G	JTS-1	muscovite	77,45	1,08E-02	0,00E+00	1,10E-03	77,12	99,6	561,08	1,17	SPA0001-11	0,00473	1,58E-06	13,268	2,54E-13
0184-01H	JTS-1	muscovite	78,02	1,13E-02	0,00E+00	2,38E-03	77,31	99,1	562,26	1,12	SPA0001-11	0,00473	1,58E-06	21,700	4,15E-13
0184-01I	JTS-1	muscovite	77,71	1,10E-02	0,00E+00	4,52E-04	77,58	99,8	563,91	1,18	SPA0001-11	0,00473	1,58E-06	25,493	4,88E-13
0184-01J	JTS-1	muscovite	77,89	1,07E-02	0,00E+00	1,22E-04	77,86	100	565,65	1,03	SPA0001-11	0,00473	1,58E-06	29,245	5,60E-13
0184-02A	JTS-1	muscovite	73,97	1,26E-02	0,00E+00	8,44E-03	71,47	96,6	525,39	5,14	SPA0001-11	0,00473	1,58E-06	0,341	6,53E-15
0184-02B	JTS-1	muscovite	80,74	1,27E-02	2,49E-03	4,78E-03	79,33	98,3	574,83	3,60	SPA0001-11	0,00473	1,58E-06	0,754	1,44E-14
0184-02C	JTS-1	muscovite	77,95	1,14E-02	0,00E+00	1,05E-03	77,65	99,6	564,33	1,48	SPA0001-11	0,00473	1,58E-06	3,272	6,25E-14
0184-02D	JTS-1	muscovite	77,59	1,12E-02	0,00E+00	9,01E-04	77,32	99,7	562,30	1,12	SPA0001-11	0,00473	1,58E-06	9,931	1,89E-13
0184-02E	JTS-1	muscovite	77,17	1,09E-02	0,00E+00	2,72E-04	77,08	99,9	560,83	1,29	SPA0001-11	0,00473	1,58E-06	19,319	3,69E-13
0184-02F	JTS-1	muscovite	77,23	1,08E-02	0,00E+00	7,02E-05	77,21	100	561,60	1,16	SPA0001-11	0,00473	1,58E-06	9,699	1,86E-13
0184-02G	JTS-1	muscovite	77,50	1,08E-02	0,00E+00	2,75E-04	77,42	99,9	562,90	1,13	SPA0001-11	0,00473	1,58E-06	7,582	1,45E-13
0184-02H	JTS-1	muscovite	77,82	1,08E-02	0,00E+00	1,88E-04	77,77	99,9	565,09	1,38	SPA0001-11	0,00473	1,58E-06	5,125	9,80E-14
0184-02I	JTS-1	muscovite	77,20	1,09E-02	0,00E+00	2,30E-05	77,19	100	561,52	1,56	SPA0001-11	0,00473	1,58E-06	2,036	3,88E-14
0184-02J	JTS-1	muscovite	78,07	1,09E-02	0,00E+00	2,84E-05	78,06	100	566,93	1,05	SPA0001-11	0,00473	1,58E-06	12,630	2,41E-13
arithmetic mean = 558,36 2,64															
stdev = 15,77															
median = 562,60 1,30															
weighted mean ± error = 563.2 ± 0.9 Ma															

The results above were obtained using Fish Canyon sanidine as the neutron fluence monitor. Five individual crystals of sanidine were irradiated from each pit, as shown in Fig. 17, and a total of 25 grains were analysed for calculating the J factor for each disk.

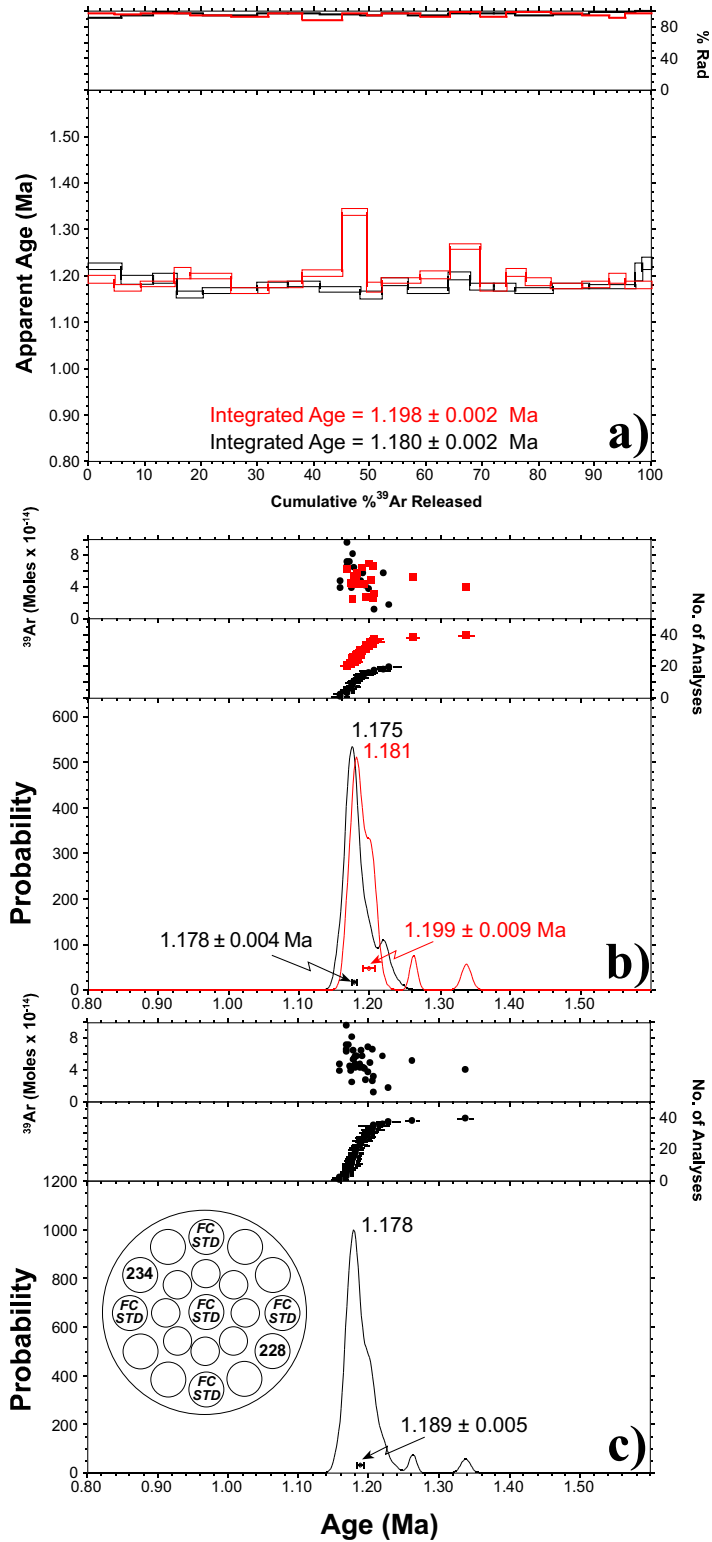


Fig. 21 – Thirty-nine single crystals of Alder Creek sanidine standards irradiated in the positions shown in Fig. 21c (insert) and analyzed by the total fusion method yield the results illustrated in (a). The total fusion results (1σ) are plotted in a cumulative % ^{39}Ar released vs. apparent age diagram, an unusual way of illustrating total fusion results, to facilitate visualizing the relative sizes of the grains (approximately proportional to the amount of ^{39}Ar released). The plot also helps visualizing the reproducibility of the results among grains of the same sample (same irradiation pit) and between samples. The results for two grains are quite distinct from the rest of the samples, possibly indicating heterogeneity in the sample or the presence of a contaminant. It is also clear from the diagrams that the results are not reproducible at the 1σ confidence level. The integrated ages (equivalent to a total fusion age and, in the absence of recoil, to the K-Ar age for the sample) calculated from the total gas yielded from each sample are 1.198 ± 0.002 and 1.180 ± 0.002 , compatible, at the 2σ confidence level, with the proposed age for these standards. The probability density plot for the results (c) illustrate a well defined age distribution with mean weighted averages for grains from each sample yielding ages of 1.178 ± 0.004 and 1.199 ± 0.009 . The mean weighted average for the entire sample is 1.189 ± 0.005 , a result entirely compatible with the accepted value for this standard (Table III).

TABLE III
Standards analyzed at USP.

Std No.	Mineral	K-Ar (Ma) $\pm 1\sigma$	$^{40}\text{Ar}/^{39}\text{Ar}$ (Ma) $\pm 1\sigma$ (published)	$^{40}\text{Ar}/^{39}\text{Ar}$ (Ma) $\pm 1\sigma$ weighted mean \pm error (error propagation according to Taylor, 1982) includes error in J (CPGeo/USP Lab)
SJ-1	muscovite	572.7 ± 10.7^b	–	563.2 ± 0.9
GA 1550	biotite	97.9 ± 0.9^a	98.8 ± 0.5^e	99.08 ± 0.15
KA-86	lepidolite	97.3 ± 3.1^b	–	97.9 ± 0.3
KA-83	orthoclase	95.4 ± 3.9^b	–	92.6 ± 0.5
P-207	muscovite	81.0 ± 2.1^c	–	82.0 ± 0.5
FC-2	sanidine	–	28.02 ± 0.16^e	[28.02]
B4M	muscovite	18.6 ± 0.4^a	–	18.53 ± 0.17
B4B	biotite	17.3 ± 0.2^a	–	17.30 ± 0.20
AC	sanidine	1.12 ± 0.02^a	1.194 ± 0.007^e 1.186 ± 0.006^f	1.189 ± 0.005

a. McDougall and Harrison, 1999. b. University of São Paulo (K-Ar ages- K-Ar laboratory, unpublished results). c. Dalrymple and Lanphere, 1969. d. Roddick, 1983. e. Renne et al., 1998. f. Turrin et al., 1994. Age in [] is the nominal age for the neutron fluence monitor used to calculate the other $^{40}\text{Ar}/^{39}\text{Ar}$ ages in the column.

USGS P-207 MUSCOVITE

The USGS P-207 muscovite was used extensively as a standard in K-Ar geochronology (Dalrymple and Lanphere 1969, p. 114–115) but has not been

used in $^{40}\text{Ar}/^{39}\text{Ar}$ geochronology. The incremental heating analysis of five grains of P-207 yield slightly disturbed spectra, none of which produces a well-defined plateau ages (Fig. 25a-f). Since instrumentation noise was no longer a factor during these

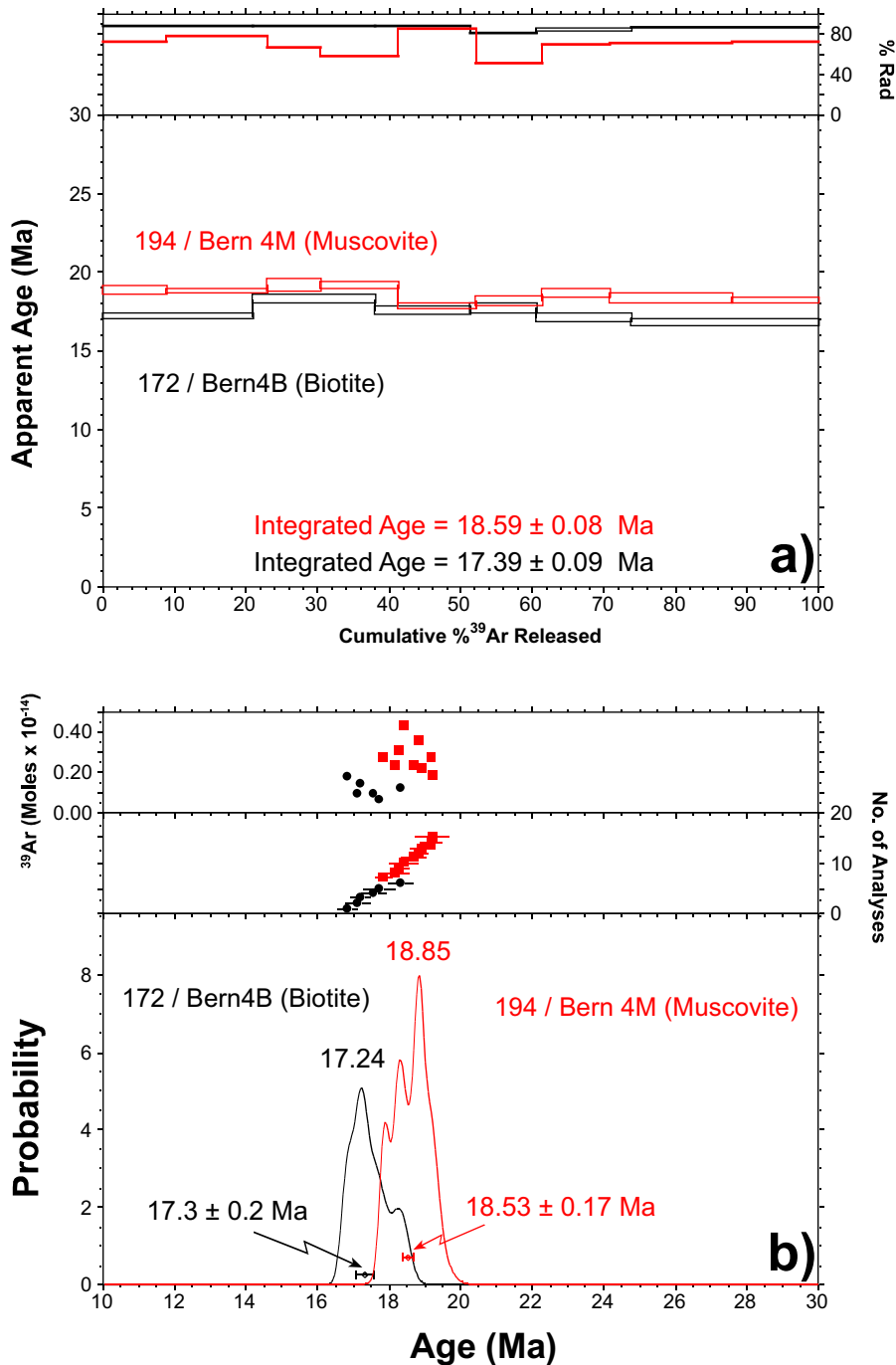


Fig. 22 – Bern 4M (muscovite) and Bern 4B (biotite) standards analyzed by the total fusion method are plotted in the cumulative %³⁹Ar released vs. apparent age diagram shown in (a). The results for each standard population are not reproducible at the 1 σ confidence level; however, the integrated ages, 17.39 ± 0.09 and 18.59 ± 0.08 Ma, are remarkably close to the proposed K-Ar ages for these standards (Table III). Probability density plots (b) for the results in (a) show some scatter but the weighted mean ages calculated for each standard is entirely consistent with the proposed ages for these minerals.

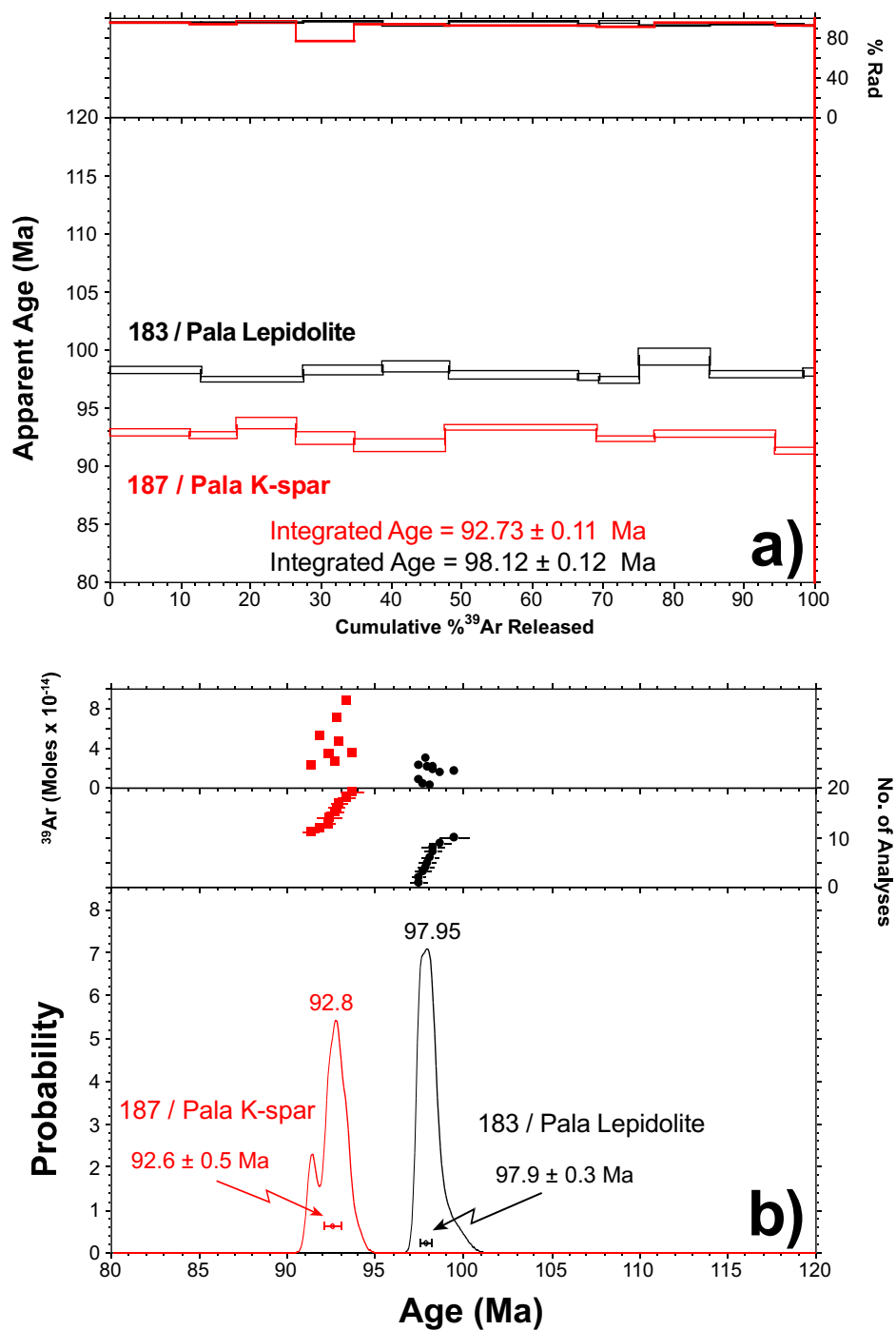


Fig. 23 – Pala KA-86 (lepidolite) and Pala KA-83 (K-spar) standards analyzed by the total fusion method are plotted in the cumulative % ^{39}Ar released vs. apparent age diagram shown in (a). The results for each standard population are not reproducible at the 1σ confidence level; however, the integrated ages, 98.12 ± 0.12 and 92.73 ± 0.11 Ma, are within 2σ from the proposed K-Ar ages for these minerals (Table III). Probability density plots (b) for the results in (a) show relatively well defined distributions; the weighted mean ages calculated for each standard is consistent with the proposed ages for these minerals at the 2σ confidence level.

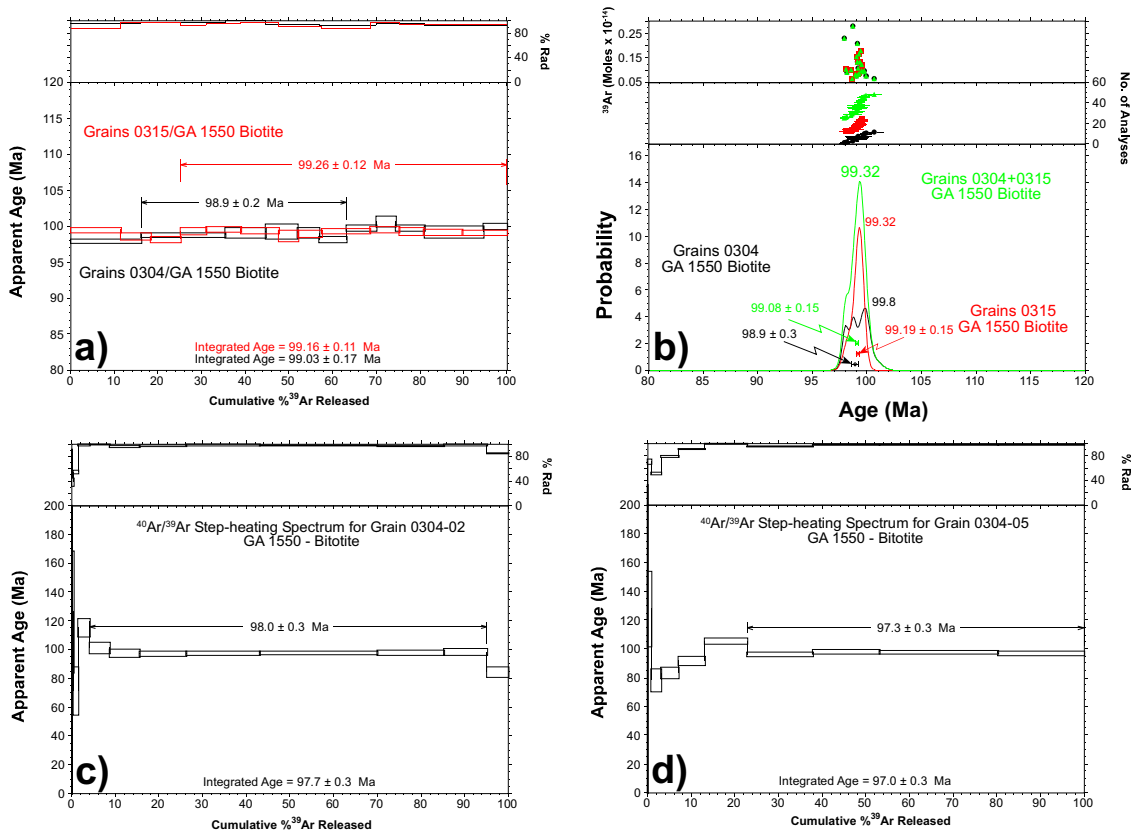


Fig. 24 – Two samples, one composed of 11 grains and the other composed of 13 grains of GA 1550 biotite crystals, irradiated in different disks, were analyzed by the total fusion method. The results, illustrated in (a) yield well defined age distributions and integrated ages compatible with the K-Ar and the proposed $^{40}\text{Ar}/^{39}\text{Ar}$ age for this standard. Ideograms plotted for each sample population yield weighted mean ages of 98.9 ± 0.3 and 99.19 ± 0.15 Ma for the two groups. An ideogram plotted for all the grains (grains 0304 + 0315) yields a high probability peak at 99.32 and a weighted mean age of 99.08 ± 0.15 Ma; the proposed age for this standard is 98.8 ± 0.5 Ma, indicating that the USP results are entirely compatible with the expected ages for the samples. Figures 24 (c) and (d) illustrate incremental heating analyses of two grains of GA 1550 biotite (each step plotted with 2σ errors). Both grains yield well-defined plateau ages, one at 98.0 ± 0.3 Ma and the other at 97.3 ± 0.3 Ma, also within 2σ confidence level for the proposed age for this standard.

analyses, the disturbed spectra may suggest that the grains may have undergone partial argon losses after precipitation or have domains susceptible to recoil losses (Fig. 25c), indicating that P-207 may not be a suitable standard for $^{40}\text{Ar}/^{39}\text{Ar}$ geochronology. A probability density plot for all the results from P-207 grains yield a broad age distribution (similar to the broad distribution in K-Ar ages obtained during an international interlaboratory comparison for P-207; Dalrymple and Lanphere 1969), but the

weighted mean $^{40}\text{Ar}/^{39}\text{Ar}$ age (82.0 ± 0.5 Ma) is compatible with the mean K-Ar age obtained for P-207 (81.0 ± 2.1 Ma) in the interlaboratory comparison.

JTS-1 MUSCOVITE

This muscovite is used as an internal standard at the USP K-Ar laboratory. Incremental-heating analysis of two grains from this standard yield the spectra illustrated in Fig. 26a and b. One grain yield two

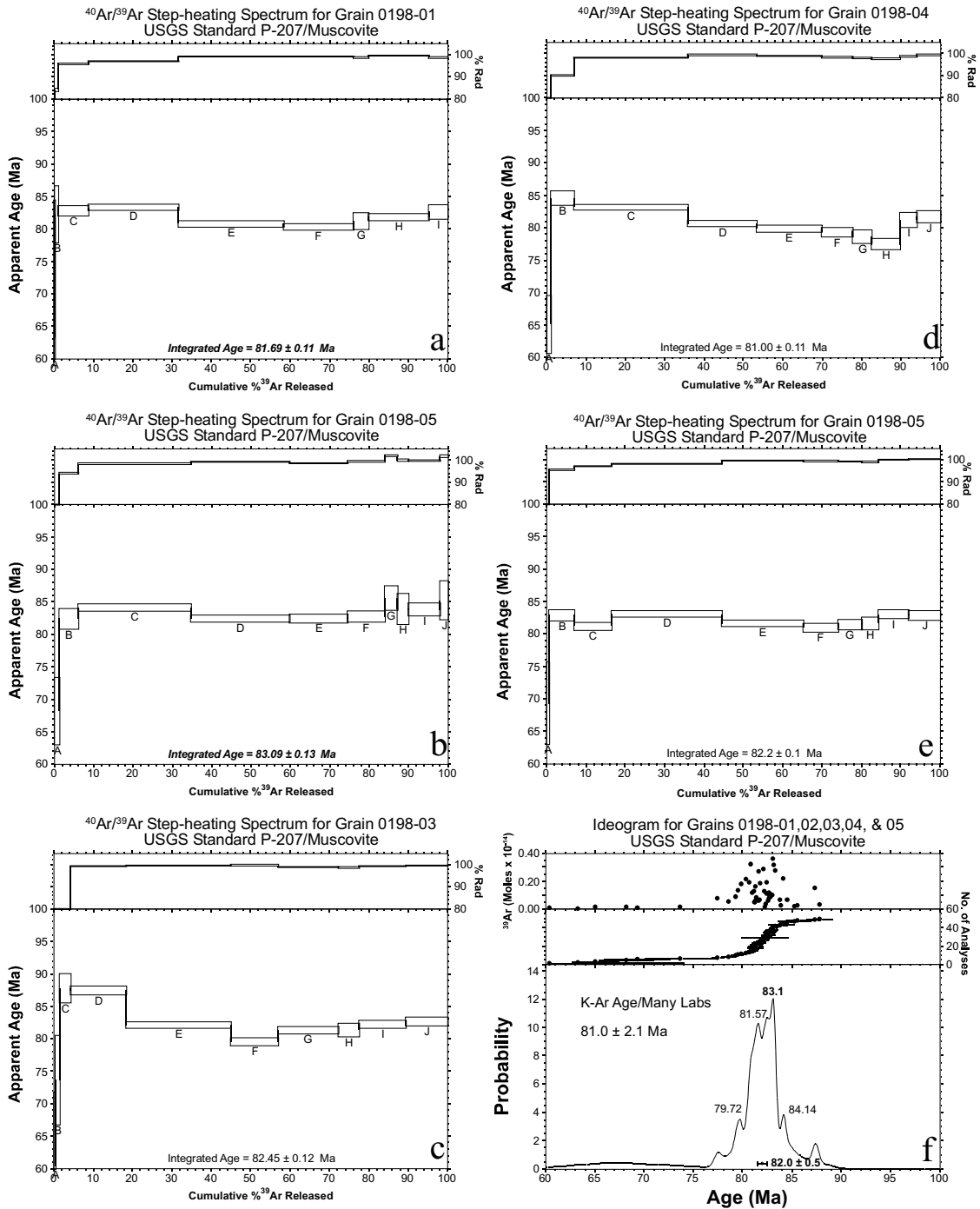


Fig. 25 – Five grains of muscovite standard P-207 analyzed by the laser incremental heating method yield disturbed spectra and fail to reach plateaus, suggesting that the samples may have been subject to partial $^{40}\text{Ar}^*$ losses. The large spread in the ideogram illustrated in (f) nevertheless yields a weighted mean age of 82.0 ± 0.5 Ma, entirely compatible with the proposed K-Ar age for this standard (81.0 ± 2.1 Ma).

plateau ages (562.9 ± 0.6 and 564.1 ± 0.7 Ma) while the other grain yield a plateau age of 562.1 ± 0.6 Ma (each individual step shows 2σ errors). The ideograms for the two grains (Fig. 26c) yield reproducible results, with weighted mean ages for the two grains of 563.2 ± 1.0 and 563.2 ± 1.4 Ma. The weighted mean age for all the analysis for the two grains [563.2 ± 0.9 Ma(1σ)] is within error from the K-Ar age, determined at the USP K-Ar laboratory, for this sample [572.69 ± 10.73 Ma].

FUTURE DEVELOPMENTS AND CONCLUSIONS

The experimental results illustrated above indicate that the Ar Laboratory at CPGeo/USP is fully operational. The instrumentation has been repeatedly tested in fully automated mode with exceptional results. Few instrumentation faults and design problems have been identified and corrected. The analyses of mass spectrometer blanks, extraction line blanks, and air aliquots reveal very low blanks, the steady maintenance of the ultra-high vacuum, and analytical parameters (beam stability, sensitivity, discrimination, etc.) suitable for modern $^{40}\text{Ar}/^{39}\text{Ar}$ geochronology.

Results from calibration tests for the nuclear reactor are extremely encouraging, indicating that the IPEN reactor is suitable for the type of irradiation necessary for modern, precise, and accurate $^{40}\text{Ar}/^{39}\text{Ar}$ geochronology. Insightful advice from reactor operators, such as the introduction of the rotational device for sample irradiation, circumvents the problem of heterogeneous neutron flux, ensuring that J-factors calculated for a sample disk are applicable to all samples in that disk, irrespective of its position in relation to the neutron fluence monitors. The J-factors obtained indicate that the flux of fast neutrons is high enough for the generation of suitable quantities of ^{39}Ar in K-bearing samples and that irradiations of 5-64 hours suffice for most geochronological applications at the reactor position currently used. The calibration tests for interfering isotope reactions at the IPEN reactor yield parameters very similar to those obtained for other reactors used in $^{40}\text{Ar}/^{39}\text{Ar}$ geochronology. We intend to

monitor these parameters for each irradiation using Ca-Si- and K-Fe-Si-glasses used in other laboratories to ascertain the precision and the accuracy of the parameters measured for the IEA-R1 nuclear reactor at IPEN/CNEN, ensuring the quality of the geochronology results obtained at the Ar Laboratory at CPGeo/USP. We also intend to investigate the irradiation of samples in a core position (position EIBE, Fig. 18), which would provide a more intense neutron flux and require shorter irradiations.

Geochronological investigations requiring total fusion and incremental-heating analysis of single grains or clusters of grains (except for grains that do not couple with Ar-ion lasers such as sanidine) can be routinely carried out at the USP laboratory. Future acquisition of a CO_2 laser, the appropriate optical components, and a new sample chamber equipped with a zinc selenide window will permit step-heating analysis of mineral grains (i.e., sanidine) that do not couple efficiently with Ar-ion lasers and which, at the present moment, can only be analyzed by the total fusion method at USP. Acquisition of a resistance furnace for temperature controlled experiments will make thermochronological studies on single grains or multiple grains from samples with a thermally complex history also possible. In addition, a resistance furnace will enable the incremental heating analysis of fine grained samples (illite, bentonite, etc.), expanding the range of applicability of the Ar Laboratory at CPGeo/USP to the study of diagenetic and low temperature metamorphic processes.

ACKNOWLEDGMENT

This work was funded by FAPESP through project 94/0678-4 “ $^{40}\text{Ar}/^{39}\text{Ar}$ methodology applied to the geodynamic evolution of Western Gondwana continent”, to Koji Kawashita and Wilson Teixeira; through PRONEX program 41.096.0899.00, “Geologia isotópica e suas aplicações na América do Sul”, to U.G Cordani and W. Teixeira; the cooperation agreement between USP and the *Instituto de Pesquisas Energéticas* (IPEN) (authorization CNEN/IPEN no. 1130/92); and FAPESP Project

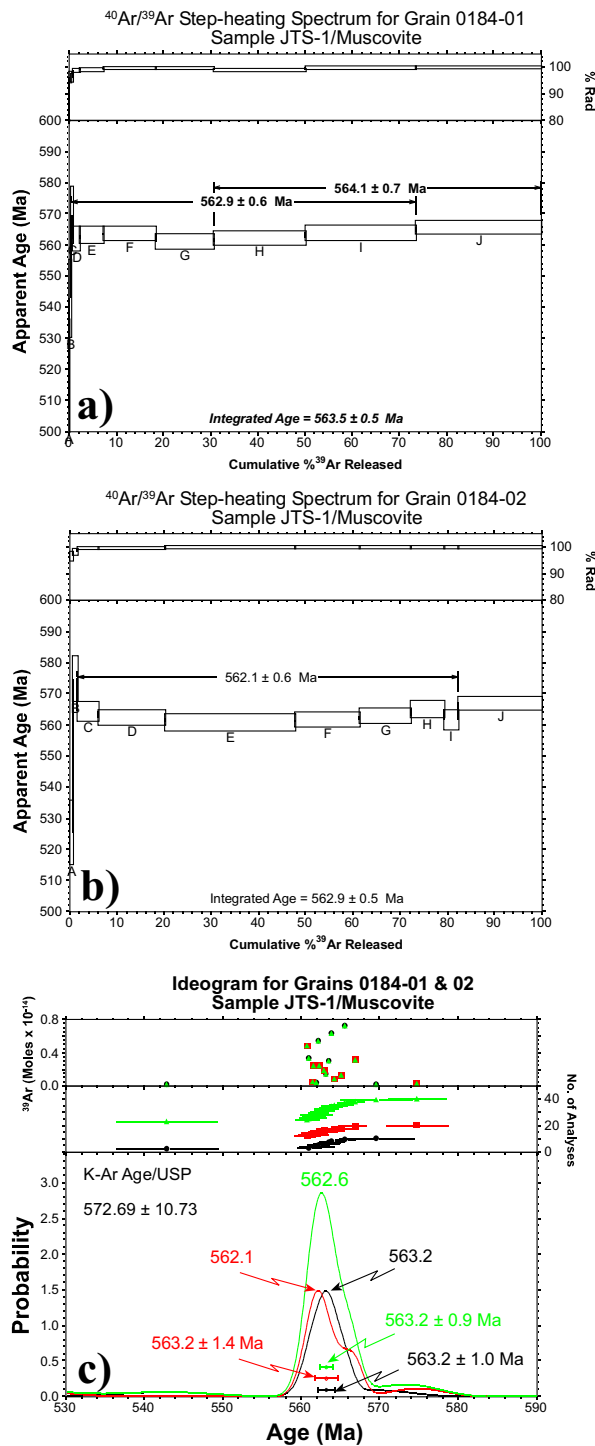


Fig. 26 – Incremental-heating analysis of two JTS muscovite crystals yield well defined plateau ages (562.9 ± 0.6 and 564.1 ± 0.7 Ma for one grain and 562.1 ± 0.6 Ma for the other) (each individual step shows 2σ errors). The ideograms for the two grains (c) yield reproducible results, with weighted mean ages for the two grains of 563.2 ± 1.0 and 563.2 ± 1.4 Ma. The weighted mean age for every step analyzed [$563.2 \pm 0.9\text{Ma}(1\sigma)$] is within error from the K-Ar age for this sample (572.69 ± 10.73 Ma).

No. 2000/04208-5 to Wilson Teixeira. The senior author is thankful to the Dean of the School of Physical Sciences and Engineering at UQ that permitted the periods of absence from the University of Queensland, and to the staff of the Berkeley Geochronology Center, Berkeley, CA, for the logistical and technical support during the execution of the project.

RESUMO

A geocronologia de $^{40}\text{Ar}/^{39}\text{Ar}$ por aquecimento a laser permite alta precisão e acurácia analítica, tem resolução espacial em escala micrométrica, e fornece um número de dados estatisticamente significantes para o estudo de processos geológicos e planetários. Um recém construído laboratório de $^{40}\text{Ar}/^{39}\text{Ar}$ no CPGeo/USP, São Paulo, Brazil, mune a sociedade científica brasileira com uma técnica eficaz aplicável aos estudos geológicos e cosmoquímicos.

Informações detalhadas sobre a montagem do laboratório, as condições ambientais, e a instrumentação instalada fornecem os parâmetros necessários para uma avaliação da adequação do laboratório do CPGeo/USP para uma diversa gama de aplicações. Detalhes sobre procedimentos analíticos, inclusive separação mineral, irradiação no reator do IPEN/CNEN na USP, e análise de espectrometria de massa permite pesquisadores interessados a elaborar procedimentos de amostragem e preparação de amostras adequados aos objetivos de seus estudos.

Finalmente, os resultados de testes de calibração usando sais e vidros de Ca e K, padrões minerais internacionais, e padrões internos mostram que a acurácia e precisão dos resultados obtidos no laboratório do CPGeo/USP são comparáveis a resultados obtidos nos melhores laboratórios internacionais. Os exaustivos procedimentos de calibração e padronização efetuados garantem que os estudos analíticos efetuados em nosso laboratório ganharão credibilidade internacional imediata, permitindo estudantes e cientistas brasileiros a conduzirem pesquisas de ponta nas áreas de ciências da terra e planetária.

Palavras-chave: geocronologia, método $^{40}\text{Ar}/^{39}\text{Ar}$, irradiação, calibração.

REFERENCES

- BRERETON NR. 1970. Corrections for interfering isotopes in the $^{40}\text{Ar}/^{39}\text{Ar}$ dating method. *Earth Planet Sci Lett* 8: 427-433.
- CULLER TS, BECKER TA, MULLER RA AND RENNE PR. 2000. Lunar impact history from $^{40}\text{Ar}/^{39}\text{Ar}$ dating of glass spherules. *Science* 287: 1785-1788.
- DALRYMPLE GB AND LANPHERE MA. 1969. Potassium-argon dating, San Francisco: Freeman, 258 p.
- DEINO A AND POTTS R. 1990. Single-crystal $^{40}\text{Ar}/^{39}\text{Ar}$ dating of the Ologesailie Formation, southern Kenya rift. *J Geophys Res* 95: 8453-8470.
- DONG H, HALL CM, PEACOR DR AND HALLIDAY AN. 1995. Mechanisms of argon retention in clays revealed by laser $^{40}\text{Ar}/^{39}\text{Ar}$ dating. *Science* 267: 355-359.
- DONG H, HALL CM, HALLIDAY AN AND PEACOR DR. 1997. Laser $^{40}\text{Ar}-^{39}\text{Ar}$ dating of microgram-size illite samples and implications for thin section dating. *Geochim Cosmochim Acta* 61: 3803-3808.
- DUNLAP WJ. 1997. Neocrystallization or cooling? $^{40}\text{Ar}/^{39}\text{Ar}$ ages of white micas from low-grade mylonites. *Chem Geol* 143: 181-203.
- GIRARD J-P AND ONSTOTT TC. 1991. Application of $^{40}\text{Ar}/^{39}\text{Ar}$ laser-probe and step-heating techniques to the dating of diagenetic K-feldspar overgrowths. *Geochim Cosmochim Acta* 55: 3777-3793.
- GOODWIN LB AND RENNE PR. 1991. Effects of progressive mylonitization on Ar retention in biotites from the Santa Rosa mylonite zone, California, and thermochronologic implications. *Contrib Mineral Petrol* 108: 283-297.
- HARRISON TM. 1981. Diffusion of ^{40}Ar in hornblende. *Contrib Mineral Petrol* 78: 324-331.
- HARRISON TM AND MCDUGALL I. 1982. The thermal significance of potassium feldspar K-Ar ages inferred from $^{40}\text{Ar}/^{39}\text{Ar}$ age spectrum results. *Geochim Cosmochim Acta* 46: 1811-1820.
- IZETT GA, DALRYMPLE GB AND SNEE LW. 1991. $^{40}\text{Ar}/^{39}\text{Ar}$ age of Cretaceous-Tertiary boundary tektites from Haiti. *Science* 252: 1539-1542.
- LEE J. 1995. Rapid uplift and rotation of mylonitic rocks from beneath a detachment fault: Insights from potassium feldspar $^{40}\text{Ar}/^{39}\text{Ar}$ thermochronology, northern Snake Range, Nevada. *Tectonics* 14: 54-77.

- McCONVILLE P, KELLEY S AND TURNER G. 1988. Laser probe $^{40}\text{Ar}/^{39}\text{Ar}$ studies of the Peace River L6 chondrite. *Geochim Cosmochim Acta* 52: 2487-2499.
- MCDUGALL I. 1981. $^{40}\text{Ar}/^{39}\text{Ar}$ age spectra from the KBS Tuff, Koobi Fora Formation. *Nature (London)* 294: 120-124.
- MCDUGALL I. 1985. K-Ar and $^{40}\text{Ar}/^{39}\text{Ar}$ dating of the hominid-bearing Pliocene-Pleistocene sequence at Koobi Fora, Lake Turkana, northern Kenya. *Geol Soc Am Bull* 96: 159-175.
- MCDUGALL I AND HARRISON TM. 1999. *Geochronology and Thermochronology by the $^{40}\text{Ar}/^{39}\text{Ar}$ Method*, 2nd ed., Oxford: Oxford University Press, 269 p.
- MERRIHUE C AND TURNER G. 1966. Potassium-argon dating by activation with fast neutrons. *J Geophys Res* 71: 2852-2857.
- NIER AO. 1940. A mass spectrometer for routine isotope abundance measurements. *Rev Sci Inst* 11: 212-216.
- ONSTOTT TC, MUELLER C, VROLIJK PJ AND PEVEAR DR. 1997. Laser $^{40}\text{Ar}/^{39}\text{Ar}$ microprobe analyses of fine-grained illite. *Geochim Cosmochim Acta* 61: 3851-3861.
- PLIENINGER T AND SCHAEFFER OA. 1976. Laser probe $^{39}\text{Ar}/^{40}\text{Ar}$ ages of individual mineral grains in lunar basalt 15607 and lunar breccia 15465. *Geochim Cosmochim Acta Suppl.* 7 (Proceedings of the Seventh Lunar Science Conference): 2055-2066.
- PODOSEK FA AND HUNEKE JC. 1973. Argon-40-argon-39 chronology of four calcium-rich achondrites. *Geochim Cosmochim Acta* 37: 667-684.
- RENNE PR. 2000. K-Ar and $^{40}\text{Ar}/^{39}\text{Ar}$ Dating. In: Noller JS et al. (Ed.), *Quaternary Geochronology: Methods and Applications*, Washington: American Geophysical Union, p. 77-100.
- RENNE PR AND BASU AR. 1991. Rapid eruption of the Siberian Traps flood basalts at the Permo-Triassic boundary. *Science* 253: 176-179.
- RENNE PR, BECKER TA AND SWAPP SM. 1990. $^{40}\text{Ar}/^{39}\text{Ar}$ laser-probe dating of detrital micas from the Montgomery Creek Formation, Northern California; clues to provenance, tectonics, and weathering processes. *Geology* 18: 563-566.
- RENNE PR, ERNESTO M, PACCA IG, COE RS, GLEN JM, PRÉVOT M AND PERRIN M. 1992. The age of Paraná flood volcanism, rifting of Gondwanaland, and the Jurassic-Cretaceous boundary. *Science* 258: 975-979.
- RENNE PR, SHARP WD, DEINO AL, ORSI G AND CIVETTA L. 1997. $^{40}\text{Ar}/^{39}\text{Ar}$ dating into the historical realm: Calibration against Pliny the Younger. *Science* 277: 1279-1280.
- RENNE PR, SWISHER CC, DEINO AL, KARNER DB, OWENS TL AND DEPAOLO DJ. 1998. Intercalibration of standards, absolute ages and uncertainties in $^{40}\text{Ar}/^{39}\text{Ar}$ dating. *Chem Geol* 145: 117-152.
- REYNOLDS PH AND MUECKE GK. 1978. Age studies on slates: Applicability of the $^{40}\text{Ar}/^{39}\text{Ar}$ step-wise outgassing method. *Earth Planet Sci Lett* 40: 111-118.
- RODDICK JC. 1983. High precision intercalibration of $^{40}\text{Ar}/^{39}\text{Ar}$ standards. *Geochim Cosmochim Acta* 47: 887-898.
- SMITH PE, EVENSEN NM AND YORK D. 1993. First successful $^{40}\text{Ar}/^{39}\text{Ar}$ dating of glauconites: Argon recoil in single grains of cryptocrystalline material. *Geology* 21: 41-44.
- SUTTER JF AND HARTUNG JB. 1984. Laser microprobe $^{40}\text{Ar}/^{39}\text{Ar}$ dating of mineral grains in situ. *Scan Elec Micros* 4: 1525-1529.
- SWISHER III CC, GRAJALES-NISHIMURA JM, MONTANARI A, MARGOLIS SV, CLAEYS P, ALVAREZ W, RENNE P, CEDILLO-PARDO E, MAURRASSE FJ-MR, CURTIS GH, SMIT J AND MCWILLIAMS MO. 1992. Coeval $^{40}\text{Ar}/^{39}\text{Ar}$ ages of 65.0 million years ago from Chicxulub crater melt rock and Cretaceous Tertiary boundary tektites. *Science* 257: 954-958.
- TURNER G. 1969. Thermal histories of meteorites by the $^{39}\text{Ar}/^{40}\text{Ar}$ method. In: MILLMAN PM (ed.), *Meteorite Research*, Reidel: Dordrecht, p. 407-417.
- TURNER G AND BANNON MP. 1992. Argon isotope geochemistry of inclusion fluids from granite-associated mineral veins in southwest and northeast England. *Geochim Cosmochim Acta* 56: 227-243.
- TURRIN BD, DONNELLY NJM AND HEARN BCJR. 1994. $^{40}\text{Ar}/^{39}\text{Ar}$ ages from the rhyolite of Alder Creek, California; age of the Cobb Mountain normal-polarity subchron revisited. *Geology* 22: 251-254.
- VASCONCELOS PM. 1999a. K-Ar and $^{40}\text{Ar}/^{39}\text{Ar}$ geochronology of weathering processes: Annual Re-

- views of Earth and Planetary Sciences 27: 183-229.
- VASCONCELOS PM. 1999b. $^{40}\text{Ar}/^{39}\text{Ar}$ Geochronology of Supergene Processes in Ore Deposits. *Reviews in Economic Geology* 12: 73-113.
- VASCONCELOS PM, BECKER TA, RENNE PR AND BRIMHALL GH. 1992. Age and duration of weathering by $^{40}\text{K}/^{40}\text{Ar}$ and $^{40}\text{Ar}/^{39}\text{Ar}$ analysis of potassium-manganese oxides. *Science* 258: 451-455.
- VASCONCELOS PM, BRIMHALL GH, BECKER TA AND RENNE PR. 1994a. $^{40}\text{Ar}-^{39}\text{Ar}$ analysis of supergene jarosite and alunite: Implications to the paleoweathering history of the western USA and West Africa. *Geochim Cosmochim Acta* 58: 401-420.
- VASCONCELOS PM, RENNE PR, BRIMHALL GH AND BECKER TA. 1994b. Direct dating of weathering phenomena by $^{40}\text{Ar}/^{39}\text{Ar}$ and K-Ar analysis of supergene K-Mn oxides. *Geochim Cosmochim Acta* 58: 1635-1665.
- YORK D, HALL CM, YANASE Y, HANES JA AND KENYON WJ. 1981. $^{40}\text{Ar}/^{39}\text{Ar}$ dating of terrestrial minerals with a continuous laser. *Geophys Res Lett* 8: 1136-1138.